EurJOC
European Journal of Organic Chemistry

Research Article
doi.org/10.1002/ejoc.202500713

Chemistry Europe
European Chemical Societies Publishing

www.eurjoc.org

VIP *Very Important Paper*

# A New Paradigm for the Supramolecular Structure of Laterally Offset Diarenes: Polymorphs II of *Para*-Substituted Acetophenone Azines, $Y_p$—Ph—(Me)C=N—N=C(Me)—Ph—$Y_p$ (Y = Cl, Br, $CH_3$)

Harmeet Bhoday, Kaidi Yang, Steven P. Kelley, and Rainer E. Glaser*

The crystal structures of polymorphs **II** of acetophenone azines $Y_p$—Ph—RC=N—N=CR—Ph—$Y_p$ with R = $CH_3$ and Y = Cl (**1M**), Br (**2M**), and $CH_3$ (**8M**) are discussed. The azine molecules in polymorphs **II** are $C_i$-symmetric with *trans*-azine moieties and conrotatory phenyl twists. Polymorphs **1M-I** and **2M-I** contain $C_2$-symmetric enantiomers with pronounced azine twists and disrotatory phenyl twists and allow for strong lateral double T-contacts. The three polymorphs **II** exemplify the new Paradigm IV for the supramolecular architectures of "laterally offset diarenes" and result in "shiplap/flat" idioteloamphiphile monolayers. Intralayer lateral attraction is provided by edge-to-face arene-arene contacts between molecules with substantial longitudinal offset and involves arene edges bridging one azine-N and one phenyl center (EAzArB synthon) or one phenyl center and substituent Y (EYArB synthon) of different neighbors. These bridging synthons are characterized by a survey of pertinent structure parameters and their structural significance is corroborated by analysis of distance mapped Hirshfeld surfaces and the computation of 2D-fingerprint plots. The edge-to-face contacts are the most attractive intermolecular interactions, and these interactions are quantified via the computed pair interaction energies and the results of aromatic analyzer analysis. Synthon binding energies and lattice energies are determined to assess polymorph preference energies.

## 1. Introduction

Azines are attracting more and more attention and two detailed reviews are available that highlight their synthesis, their structures, and their impact on diverse fields.[1,2] The classic route for making azines involves condensation of hydrazine with carbonyl compounds but modern synthetic routes offer better yields of the desired azines. Notably, new methods such as nickel-catalyzed pathways[3] and iminyl radical N—N bond cross-coupling[4] have enabled more efficient access to both symmetrical and unsymmetrical azines. In the area of pharmaceuticals, azines stand out for their wide-ranging bioactivity, including antimicrobial, antifungal, and anticancer effects.[5] Interest in azines has also grown within materials science: Azine-linked covalent organic frameworks are emerging as electrode materials for energy storage,[6] and fluorescent azines are valued for their unique optical and electrochemical behaviors.[7] We have been interested in the development of azine materials for nonlinear optics (NLO).

The successful fabrication of materials for NLO applications[8–10] rests on the central paradigm of avoiding centrosymmetry. Most organic NLO materials are polar donor-acceptor substituted conjugated molecules or polymers and the alignment of their NLO chromophores usually is marginal and may require electric field alignment. There are few examples of NLO active molecules that crystallize with near perfect or even perfect dipole parallel alignment. We have succeeded in making highly dipole parallel aligned (HDPA) organic crystals using acetophenone azines and, more recently, we also became interested in highly dipole aligned oligopeptide crystalline nanomaterials.[11,12]

We have been able to fabricate crystals with perfect dipole alignment with several unsymmetrical donor-acceptor substituted 1,4-diphenyl azine series $X_p$—Ph—RC=N—N=CR—Ph—$Y_p$, the (R, X, Y)-azines. Initial success came with the methoxy series of acetophenone azines (R = Me) with X = $OCH_3$ and Y = Cl,[13] Br,[14] I,[15] and their crystal structures are shown in **Figure 1**. Our approach aims to create polar layers of parallel aligned azines and their polar stacking in the third direction. This concept also was successfully implemented for several representatives of the phenoxy series (R = Me, X = $OC_6H_5$, Y = F, Cl, Br, I)[16–22] and the decyloxy

*H. Bhoday*
*Department of Chemistry*
*Cornell College*
*Mount Vernon, IA 52314, USA*

*H. Bhoday, R. E. Glaser*
*Department of Chemistry*
*Missouri University of Science and Technology*
*Rolla, MO 65409, USA*
*E-mail: glaserr@umsystem.edu*

*K. Yang, S. P. Kelley*
*Department of Chemistry*
*University of Missouri*
*Columbia, MO 65211, USA*

*R. E. Glaser*
*Department of Material Science and Engineering*
*Missouri University of Science and Technology*
*Rolla, MO 65409, USA*

*Supporting information for this article is available on the WWW under https://doi.org/10.1002/ejoc.202500713*

Research Article
doi.org/10.1002/ejoc.202500713

Chemistry Europe
European Chemical Societies Publishing

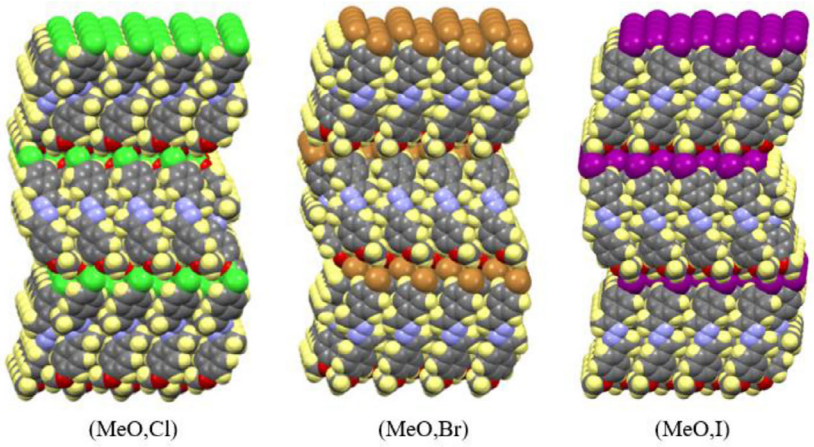


**Figure 1.** Near-perfect dipole alignment by polar stacking of polar layers.

series (R = Me, X = $O(CH_2)_9CH_3$, Y = F, Cl, Br).[23–26] Furthermore, we recently reported on the methoxyphenyl series of acetophenone azines MeO—Ph—Ph—(Me)C═N—N═C(Me)—Ph—$Y_{para}$ (Y = F, Cl, Br, I),[27–31] which are formed by combination of one halogen substituted acetophenone, O═C(Me)—Ph—$Y_p$, and one methoxy-substituted 4-acetylbiphenyl, MeO—Ph—Ph—(Me)C═O.[32,33]

The key concept guiding the fabrication of these HDPA materials consists in the use of lateral quadrupole–quadrupole interactions to compensate and overcome the electric repulsion associated with dipole–dipole parallel alignment.[34–36] While our primary interest has been with unsymmetrical (R, X, Y)-azines, we have also studied the symmetrical (R, Y, Y)-azines intensively to gain an understanding of their molecular stereochemistry[37–39] and their intermolecular interactions in their crystals.[40] We have previously discussed possible arrangements of idioteloamphiphile monolayers (IAM) and beloamphiphile monolayers (BAM),[23,34] and several options are depicted in **Scheme 1**. Idioteloamphiphiles contain two polar head groups of the same kind (Greek, idios) at the ends (Greek, telos) of a nonpolar chain. Beloamphiphiles have different head groups at the ends of a conjugated spacer, and the prefix belo (Greek, belos, arrow) reflects that beloamphiphiles are polar. A symmetrical azine is schematically represented by five units, which represent the halogen (green), the arenes (grey), and the azine bridge (blue). An unsymmetrical azine also features an alkoxy group (red). We have discussed several IAM types in the previous article[40] and the ones that matter in this article are ideal-shiplap/flat, which feature ideal-shiplap motif in one longitudinal offset direction (LOS1) and flat motif in the perpendicular direction (LOS2).

Here we are interested in the symmetrical *para*-chloroacetophenone azine **1**(Me, Cl, Cl), its bromo analog **2**(Me, Br, Br), and its methyl analog **8**(Me, Me, Me), and for brevity we refer to these acetophenone azines (R = Me) as **1M**, **2M**, and **8M**, respectively. We reported polymorphs **I** of **1M**[41] and **2M**[42] several years ago,[43] and a detailed analysis of the crystal architecture of **1M-I** led us to the discovery of the crystal environment induced symmetry reduction (CEISR).[40] We have recently succeeded in the crystallization of polymorphs **1M-II**[44] and **2M-II**[45] and their structures are discussed in comparison to their polymorphs **I** with focus on layer morphology and acetophenone azine stereochemistry. Polymorphs **II** feature the "ideal-shiplap" motif, that is, an IAM with alternating offset in one layer direction (LOS1) and it is "ideal" because LOS1 = 1/2 m (Scheme 1). The concept of shiplap IAMs is not limited to chloroazine **1M** and bromoazine **2M** but is realized by a variety of symmetrical azines. **Table 1** in our recent article[40] listed IAM types of 16 crystal structures of ten symmetrical azines and that previous discussion focused on "flat" crystal structures and the occurrence of CEISR. The present Table 1 is a shortened version and informs about azine dihedral angles $\tau$. The azine in **1M-I** features a pronounced azine twist ($\tau = 134.7°$) while it is not twisted in **1M-II** ($\tau = 180°$). The bromoazine **2M** also realizes two analogous polymorphs **2M-I** ($\tau = 131.9°$) and **2M-II** ($\tau = 180°$). For azines **4M** (Y = OH),[46] **6M** ($Y = CF_3$),[47] **7M** (Y = F), **8M** (Y = Me), and **9M** ($Y = NO_2$),[48] only shiplap structures are known, and polymorphs **8M-I** (**A**, $\tau = 142.8°$) and **8M-II** (**B**, $\tau = 180°$) of *para*-methylacetophenone azine[49] are a unique set of two shiplap polymorphs. With polymorphs **I** and **II** of acetophenone azines **1M**, **2M**, and **8M** we are in a unique position to perform comparative analysis of three pairs of polymorphs of *para*-substituted acetophenone azines with focus on their isostructural polymorphs **II**. Comparisons to the crystal structures of the respective *para*-substituted (H, Y, Y) benzaldehyde azines **1H**[50,51] and **2H**[52] also is made.

Here we report on the structure and properties of the isostructural polymorphs **II** of the symmetrical *para*-chloroacetophenone azine **1M** and **2M**. Our theoretical analysis[53] of the conformational preferences of the free acetophenone azines **1M**, **2M**, and **8M** and of the corresponding benzaldehyde azines **1H**, **2H**, and **8H** provides a reference for the discussion of the conformations found in the crystals. The analysis of the crystal structures begins with a deep analysis of **1M-II** and reveals several new synthons contributing to intra- and interlayer interactions. Interaction inventory analyses are performed for the three polymorph **II** crystals and intermolecular interactions are compared quantitatively based on contact distances, machine learning assisted arene–arene interactions, and on graphical products of Hirshfeld analyses. Crystal

Research Article
doi.org/10.1002/ejoc.202500713

Chemistry Europe
European Chemical Societies Publishing

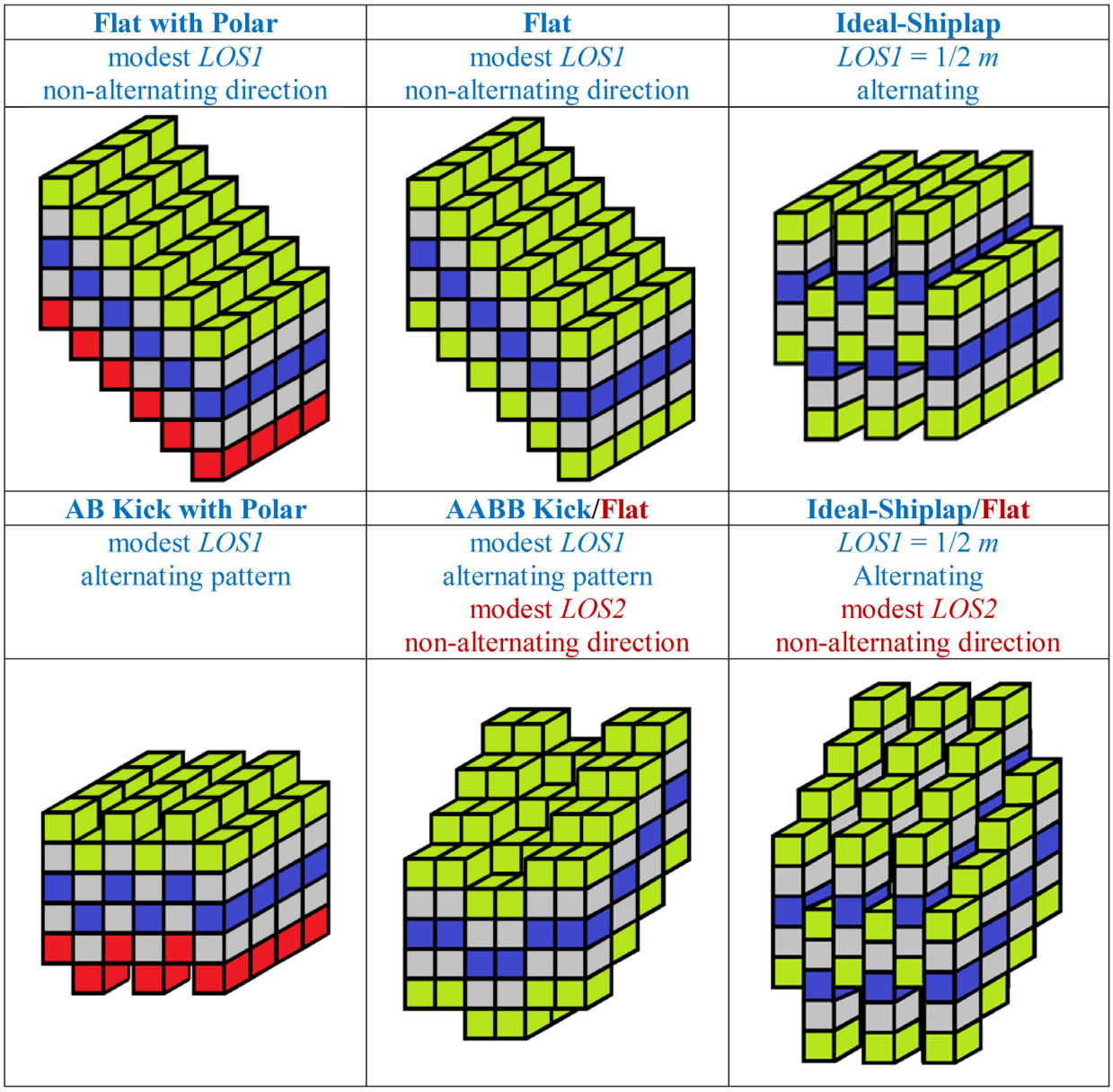


**Scheme 1.** Selected types of longitudinal offsets in BAMs and IAMs.

stabilization energies are reported which are based on the determination of next-neighbor interactions (azine stabilization energies) and lattice energies. Both ab initio and force-field methods are employed, and experimental insights allow for judgement about their validity. These data allow for an analysis of lattice energies of polymorphs **II** as a function of substituent **Y** and for the calculation of polymorph preference energies (PPEs).

## 2. Experimental and Computational Section

### 2.1. Synthesis and Crystallization of 1M and 2M

Chloroazine **1M** was synthesized by refluxing the acidic ethanolic solution of *p*-chloroacetophenone with hydrazine hydrate in a molar ratio 2:1 for 24 h. The reaction was monitored by thin layer chromatography (TLC). The resultant precipitates were collected by filtration, washed with cold ethanol, and then dried under vacuum. The product was characterized and tested for purity using $^{1}$H and $^{13}$CNMR (Figure S1 and S2, Supporting Information). The product yield for this reaction was 92%. Single crystals of polymorph **I** were grown via vapor diffusion method using chloroform as a solvent and hexane as the antisolvent. While the single crystals of polymorph **II** were grown via slow evaporation method using toluene as a solvent. The color of the two forms differed significantly, form **1M-I** was pale yellow while form **1M-II** was intense yellow.

The synthesis of bromoazine **2M** was achieved by refluxing *p*-bromoacetophenone (2 mol) with hydrazine hydrate (1 mol), 3–4 drops of acetic acid (catalyst), and 20 mL ethanol solution for 24 h. The reaction progress was tracked using TLC. The

**Table 1.** Overview of IAM types of symmetrical (R, Y, Y)-Azines with R = Me.

| # | Y | CCDC Code | CCDC #s[a)] | Temp. [K] | IAM Type | Azine twist | Ph1 twist | Ph2 twist | Sym. | CEISR | References |
|---|---|---|---|---|---|---|---|---|---|---|---|
| **1M-Ia** | Cl | LIKHUI | 1207287 | 295 | AABB kick/flat | 134.71 | −29.31 | −30.53 | $C_1$ | YES | *JOC*, 1994 ref. [38] |
| **1M-Ib** | Cl | LIKHUI02 | 2251374 | 100 | AABB kick/flat | 134.77 | −28.96 | −31.70 | $C_1$ | YES | *CEC*, 2023 ref. [40] |
| **1M-II** | Cl | LIKHUI01 | 2027206 | 100 | Ideal-shiplap/flat | 180.00 | −26.37 | 26.37 | $C_i$ | NO | This work |
| **2M-Ia** | Br | LIKJEU | 1207288 | 295 | AABB kick/flat | 131.85 | −20.96 | −27.26 | $C_1$ | YES | *JOC*, 1994 ref. [38] |
| **2M-Ib** | Br | LIKJEU03 | 2241667 | 100 | AABB kick/flat | 132.07 | −29.39 | −29.85 | $C_1$ | YES | *CEC*, 2023 ref. [40] |
| **2M-Ic** | Br | LIKJEU01 | 2056546 | 150 | AABB kick/flat | 131.85 | −29.19 | −29.70 | $C_1$ | YES | This work |
| **2M-II** | Br | LIKJEU02 | 2234130 | 150 | Ideal-shiplap/flat | 180.00 | −26.33 | 26.33 | $C_i$ | NO | This work |
| **3M** | I | LIZNEN | 139916 | 173 | Flat/flat-zigzag | 141.82 | −8.07 | −8.07 | $C_2$ | NO | *JCC*, 1999 ref. [63] |
| **4M** | OH[b)] | BITTIH | 1111781 | 295 | Shiplap/ideal-flat | 148.37 | 19.57 | 12.82 | $C_1$ | YES | *JCS PT2*, 1995 ref. [46] |
| **6M** | $CF_3$ | WEWMET | 1843926 | 173 | Shiplap/double flat | 114.38 | −2.34 | 10.42 | $C_1$ | YES | *CSD*, 2018 ref. [47] |
| **7M** | F | LIKHOC | 1207286 | 295 | ABB/shiplap | 137.99 | 1.87 | −18.61 | $C_1$ | YES | *JOC*, 1994 ref. [38] |
| **8M-I**[c)] | Me | PIYYAX | 1235041 | 295 | ABB/shiplap | 142.76 | 0.45 | −19.89 | $C_1$ | YES | *ACIEE*, 1994 ref. [49] |
| **8M-II**[c)] | Me | PIYXOK | 1235039 | 295 | Ideal-shiplap/flat | 180.00 | −23.75 | 23.75 | $C_i$ | NO | *ACIEE*, 1994 ref. [49] |
| **9M-Ia** | $NO_2$ | ZEHJUR | 1310588 | 295 | AABB shiplap/flat | 152.00 | 1.21 | 13.98 | $C_1$ | YES | *JCS PT2*, 1995 ref. [46] |
| **9M-Ib** | $NO_2$ | ZEHJUR02 | 984384 | 130 | AABB shiplap/flat | 155.22 | −0.93 | 12.34 | $C_1$ | YES | *JCS*, 2015 ref. [48] |
| **9M-II** | $NO_2$ | ZEHJUR01 | 984383 | 140 | Shiplap/flat | 113.37 | 2.0 | 11.78 | $C_1$ | YES | *JCS*, 2015 ref. [48] |

[a)]Compound numbers differentiate Y substituents and "M" indicates R = Me. [b)]Crystallized as hydrate. [c)]In ref. [49] polymorphs **8M-I** and **8M-II**, respectively, were referred to as **A** and **B**, respectively.

precipitate formed were filtered, thoroughly washed with cold ethanol, and dried under vacuum conditions. The product's structure and purity were analyzed using $^1$H and $^{13}$CNMR spectroscopy (Figure S3 and S4, Supporting Information). The reaction yield was 86%. Single crystals of polymorph **2M-I** were grown using the slow evaporation technique, employing a mixture of hexane and ethyl acetate (4:1). Polymorph **2M-II** crystals, on the other hand, were prepared through a slow evaporation process using toluene as the solvent. The two polymorphs displayed distinct colors, with polymorph **2M-I** appearing white and polymorph **2M-II** having a yellow coloration.

### 2.2. Crystal Structure Refinement

Crystal data, data collection and structure refinement details are summarized in **Table 2**. Single crystal X-ray diffraction (SCXRD) data for **1M-II** and **2M-II** were collected on a Bruker X8 Prospector diffractometer equipped with a charge coupled device (CCD) area detector using Cu Kα radiation ($\lambda = 1.54178$ Å) from a microfocus source. A hemisphere of data was collected using strategies of scans about the omega and phi axes. The crystal was cooled to −173 °C during collection using an Oxford Cryostream 700 cyrostat (Oxford Cryosystems, Oxford, UK). Unit cell determination and data reduction for polymorphs **1M-II** and **2M-II**, were performed using the Bruker Apex3 software suite.[54] The structure was solved by an iterative dual space approach as implemented in SHELXT,[55] and all nonhydrogen atoms were refined using SHELXL-2017, implemented with the Olex2 graphical user interface.[56] Nonhydrogen atoms were located from the difference map and refined anisotropically by full matrix least squares refinement against $|F^2|$. Hydrogen atoms were placed in calculated positions and constrained to ride on the carrier atoms. Methyl group hydrogen atoms were refined using a riding-rotating model. The most important structural parameters are collected in Table 2. Details of crystallographic data can be found in supporting information. CCDC codes are provided in Table 1. Crystals of polymorph **1M-I** were analyzed at two temperatures and **1M-Ib** will be compared to **1M-II** at the common temperature of 100 K. Crystals of polymorph **2M-I** were analyzed at three temperatures and **2M-Ic** will be compared to **2M-II** at the common temperature of 150 K.

### 2.3. Computational Methods for Crystal Structure Analysis

Our analyses of the crystal structures employed several publicly available softwares to evaluate relative stabilities of polymorphic crystals and to quantify and visualize intermolecular interactions.

The CrystalExplorer software was employed to calculate lattice energies $E_{lat}$ using pair interaction energies derived from molecular electron densities, which were computed at the B3LYP/6-31G(d,p) level,[57,58] and the resulting energies are commonly known as CE-B3LYP model energies. The lattice energies $E_{lat}$ are computed by direct summation of interaction energies of a central molecule **A** with its neighboring molecules $\mathbf{B}_i$ and the size of the environment is increased until $E_{lat}$ is converged to better than ≈0.25 kcal mol$^{-1}$. The cutoff is based on the separation of molecular centroids $r_{AB}$, and for our calculations $r_{AB}$ was set to 25 Å for all the crystal structures. The positions of hydrogen atoms are usually not directly determined in the X-ray diffraction experiment. In CrystalExplorer, hydrogen atoms are typically positioned based on the surrounding atoms and their expected bonding geometry, they are often calculated and refined based on chemical intuition, and sometimes their positions are further optimized using computational methods. Along these lines we computed partially optimized structures (POS) of the crystal structures **1M-I**, **1M-II**,

Research Article
doi.org/10.1002/ejoc.202500713





**Table 2.** Experimental details.

| Crystal data | Polymorph **1M-Ib** | Polymorph **1M-II** | Polymorph **2M-Ic** | Polymorph **2M-II** | Polymorph **8M-I** | Polymorph **8M-II** |
|---|---|---|---|---|---|---|
| Chemical formula | $C_{16}H_{14}Cl_2N_2$ | $C_{16}H_{14}Cl_2N_2$ | $C_{16}H_{14}Br_2N_2$ | $C_{16}H_{14}$ $Br_2N_2$ | $C_{18}H_{20}N_2$ | $C_{18}H_{20}N_2$ |
| $M_r$ | 305.19 | 305.19 | 394.11 | 394.11 | 305.19 | 305.19 |
| Crystal system, space group | Monoclinic, $P2_1/c$ | Monoclinic, $P2_1/n$ | Orthorhombic, Pbca | Monoclinic, $P2_1/n$ | Monoclinic, $P2_1/n$ | Monoclinic, $P2_1/c$ |
| Temperature [K] | 100 | 100 | 150 | 150 | 295 | 295 |
| $a$ [Å] | 15.0686(6) | 5.3766(3) | 9.3280(11) | 5.5678(2) | 11.4392(10) | 5.6140(20) |
| $b$ [Å] | 9.1426(4), | 8.7055(5) | 10.3409(12), | 8.7473(4) | 7.6147(4) | 8.7700(20) |
| $c$ [Å] | 10.3068(4) | 15.6819(8) | 30.273(4) | 15.6491(7) | 17.7270(20) | 15.736(5) |
| $\beta$ [°] | 93.7551(13) | 99.722(2) | 90.000 | 98.8027(14) | 92.289(4) | 98.060(20) |
| $V$ [Å$^3$] | 1416.88(10) | 723.47(7) | 2920.1(6) | 753.18(6) | 1542.9 | 767.105 |
| $Z$ | 4 | 2 | 8 | 2 | 4 | 2 |
| Radiation type | Mo Kα | Cu Kα | Mo Kα | Cu Kα | – | – |
| $\mu^{-1}$[mm$^{-1}$] | 0.448 | 3.946 | 5.543 | 6.743 | – | – |
| Crystal size [mm] | 0.18 × 0.10 × 0.04 | 0.26 × 0.22 × 0.13 | 0.65 × 0.10 × 0.08 | 0.40 × 0.10 × 0.07 | – | – |
| $T_{min}$, $T_{max}$ | 0.704, 0.746 | 0.614, 0.754 | 0.665, 0.123 | 0.650, 0.173 | – | – |
| No. of measured, independent and observed [$I \geq 2\sigma(I)$] reflections | 39 680, 4325, 3633 | 12 417, 1432, 1426 | 55 120, 3670, 3035 | 12 187, 1516, 1510 | – | – |
| $R_{int}$ | 0.0345 | 0.0217 | 0.0528 | 0.0282 | – | – |
| $R[F^2 > 2\sigma(F^2)]$, $wR(F^2)$, $S$ | 0.0543, 0.0865, 1.138 | 0.0243, 0.0639, 1.057 | 0.0408, 0.0667, 1.07 | 0.0215, 0.056, 1.119 | 0.06, 0.06 | 0.065, 0.065 |
| No. of parameters | 223 | 92 | 183 | 92 | – | – |
| Maximum/minimum residual electron density | 0.498, −0.283 | 0.296, −0.173 | 0.434, −0.457 | 0.273, −0.567 | – | – |

**2M-II**, **8M-I**, and **8M-II** in which we held the positions of heavy atoms and the unit cell parameters fixed and only optimized the hydrogen positions. These optimizations were performed with the 3-21G basis set and the Cartesian coordinates of these POS/3-21G structures are provided in supporting information. The unit cell of **2M-I** contains eight molecules and even the partial optimization far exceeded available computer resources.

The software CSD-Mercury was employed to calculate lattice energies based on the UNI intermolecular potentials.[59] While these force-field calculations are approximate due to their reliance on empirical pair-potential parameters, they provide a rapid assessment of the relative influence of dimers within the structure.

The CSD-Mercury software also was employed for the evaluation of aromatic interactions.[60] Pertinent intermolecular contacts were visualized in the CrystalExplorer software by generation of Hirshfeld surfaces and Hirshfeld 2D-fingerprint plots.[61]

## 3. Results and Discussion

### 3.1. Azine Conformation

#### *3.1.1. Conformation in Crystals*

Azine **1M** crystallizes with a monoclinic unit cell in space groups $P2_1/c$ and $P2_1/n$ for forms **I** and **II**, respectively. The unit cell of **I** comprises of four molecules while that of **II** contains only two molecules. Each polymorph contains one unique molecule, and the oak ridge thermal ellipsoid plot (ORTEP) representation of the molecular structure of **1M** in polymorph **II** is illustrated in the top row of **Figure 2**. Azine **2M** crystallizes with different space groups for polymorph **I** (orthorhombic, Pbca) and **II** (monoclinic, $P2_1/n$). Polymorphs **I** and **II** feature eight and two molecules, respectively, in their unit cells. Each polymorph contains only one unique molecule. The ORTEP diagram for polymorph **II** of **2M** is provided in the center row of Figure 2. The respective molecular structures of polymorph **II** of **8M** are included in the bottom row of Figure 2.

Two major differences between **1M-I** and **1M-II** concern conformational twists. The azine twist, the torsion angle $\tau = \angle$(C═N─N═C) is 134.7° in **1M-I** but it is 180° in **1M-II**. The second significant difference concerns the relative directions of the phenyl twist $\phi_1 = \angle$(C7─C2─C1═N1) and $\phi_2 = \angle$(C15─C10─C9═N2). In **1M-I**, the phenyl twists are disrotatory and the dihedral angles $|\phi_1| = 29.31°$ and $|\phi_2| = 30.53°$ have the same sign. In **1M-II**, the phenyl twists are conrotatory because the dihedral angles $\phi_1 = +26.39°$ (*P* helicity) and $\phi_2 = -26.39°$ (*M* helicity) have opposite sign and this is well illustrated by the Newman projection down the N─N bond (Figure 2).

A summary of the helicities and the conformations of polymorphs of **1M**, **2M**, and **8M** is provided in **Table 3**. In polymorphs **I** of **1M**, **2M**, and **8M**, the three twist angles cooperate to minimize $\omega$, the angle between the best planes of the arenes, to $\omega$(**1M-I**) = 70.09°, $\omega$(**2M-I**) = 67.6°, and $\omega$(**8M-I**) = 58.9°.

Research Article
doi.org/10.1002/ejoc.202500713

Chemistry Europe
European Chemical Societies Publishing

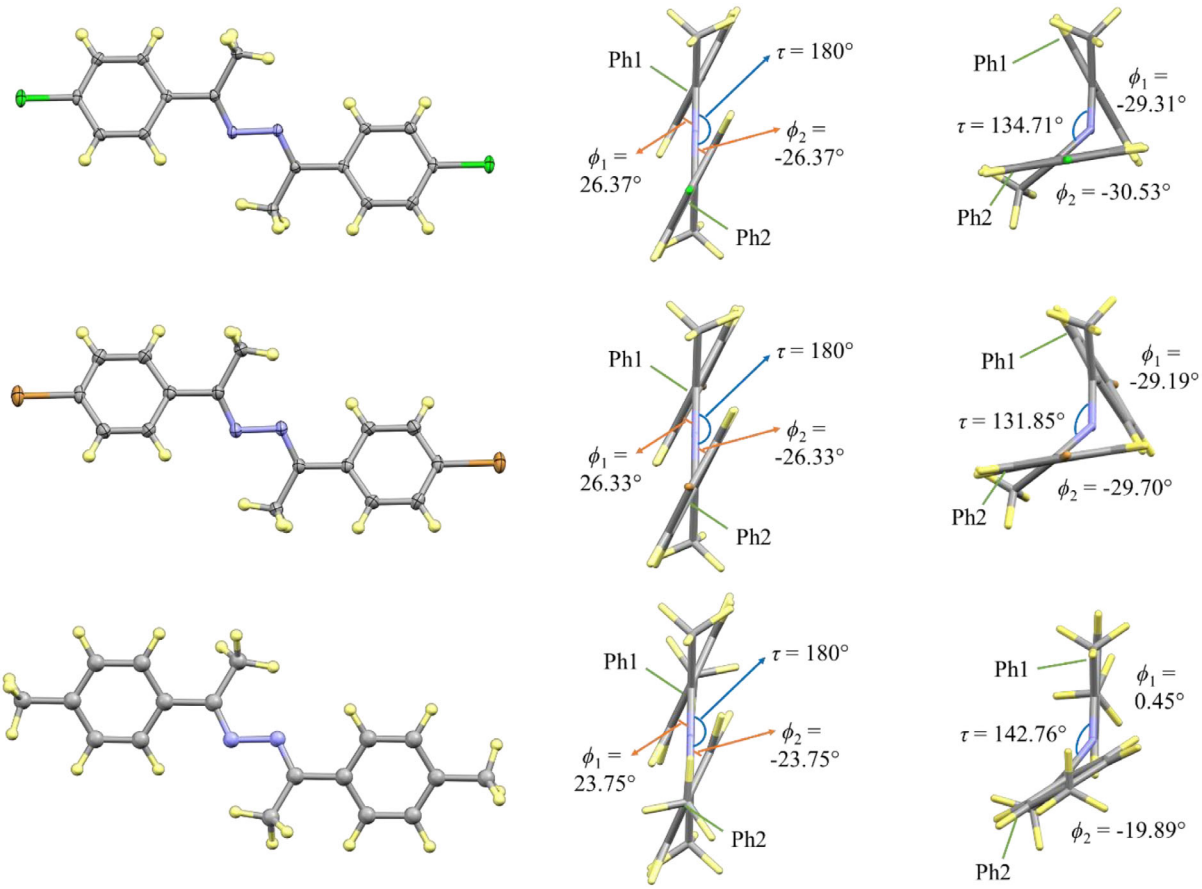


**Figure 2.** Molecular models of the crystal structures of *(E,E)*-configurated (Y, Y)-substituted acetophenone azines in polymorphic form **II** with the Newman projection on the right showing the Ph twists. Top: **1**(Me, Cl, Cl) azine **1M-II**; center: **2**(Me, Br, Br) azine **2M-II**; and bottom: **8**(Me, Me, Me) azine **8M-II**. For direct comparison, the Newman projections of the respective previously reported polymorphs **I** are displayed in the right column.

In polymorphs **II** of the three azines, the arenes are coplanar ($\omega = 0°$) and the phenyl twist controls the distance between the arene planes (Figure 2).

### 3.1.2. Conformation in the Gas-Phase

We recently described the conformational preferences (N—N, (N)C—Ph, Ph—Me) of the free azines and explained the origins of these preferences.[53] A brief overview of the conformation about the azines's N—N bond is provided in **Figure 3** and models of some pertinent stationary structures are shown in **Figure 4**.

The scans of the potential energy surfaces (PES) of the six azines as a function of dihedral angle $\tau$ include four PES regions. Region 1 includes the minima of benzaldehyde azines **1H**, **2H**, and **8H** without azine twist (*trans*, $\tau = 180°$). Region 2 includes the minima of acetophenone azines **1M**, **2M**, and **8M** with azine twists $\tau \approx 130°$. Region 3 includes structures of acetophenone azines without azine twist. Unbound shallow minima with cisoid azine conformations and $\tau \approx 80°$ occur in Region 4. The stationary structures in Regions 1–3 and their relative energies are shown in Figure 4.

The enantiomers with *P* helicity about the azine N—N bond are displayed in Figure 4 and both of their phenyl twists feature *M* helicity. Driving the dihedral $\tau$ starting from a transoid twisted azine retains the directions of the phenyl twists well beyond $\tau = 180°$. In the $C_i$-structures, the phenyl twists are conrotatory and of opposite sign as in Figure 2. Note that $C_i$-**1M** and $C_i$-**2M** are shallow transition state structures (STS) and $C_i$-**8M** corresponds to a shallow minimum (SM) on their PES. In gas phase, *trans*-azines without phenyl twists correspond to higher order saddle points. The subscripts for the *para*-methyl substituted azines **8** describe the toluene moieties' methyl conformation. These methyl groups always are staggered with one C—H bond almost perpendicular to the arene plane. In $\mathbf{8H_{apa}}$ and $\mathbf{8M_{apa}}$, the perpendicular C—H bonds of the two toluene moieties are antiparallel aligned. In $\mathbf{8M_{mg}}$, one of the perpendicular C—H bonds points into the inner groove (ig) and the other points into the outer groove (og).

## 3.2. Packing Paradigms for Laterally Offset Diarenes

The spacer in diarenes of the types $X_{para}$—Ph—RC═E—E═CR—Ph—$Y_{para}$ (E = N: azines; E = CH: butadienes) are *trans* or transoid about the central E—E bond and therefore necessarily provide lateral offset between the two arenes, i.e., the C—Ph bonds are not collinear. The question is how to best

Research Article
doi.org/10.1002/ejoc.202500713

Chemistry Europe
European Chemical Societies Publishing



**Table 3.** Azine twists ($\tau$) and phenyl twists ($\phi_1$ and $\phi_2$), and resulting Helicity in polymorphs of **1M**, **2M**, and **8M**.

| Molecule[a,b] | 1M-I | 1M-I* | 1M-II | 2M-I | 2M-I* | 2M-II | 8M-I | 8M-I* | 8M-II |
|---|---|---|---|---|---|---|---|---|---|
| Helicity | *P* | *M* | Undef. | *P* | *M* | Undef. | *P* | *M* | Undef. |
| $\tau$ | 134.71 | −134.71 | 180 | 131.85 | −131.85 | 180 | 142.76 | −142.76 | 180 |
| Conf. | +ac | −ac | Anti | +ac | −ac | Anti | +ac | −ac | Anti |
| Helicity | *M* | *P* | *P* | *M* | *P* | *P* | *P* | *M* | *P* |
| $\phi_1$ | −28.96 | 28.96 | 26.39 | −29.19 | 29.19 | 26.33 | 0.45 | −0.45 | 23.75 |
| Conf. | −sp | +sp | +sp | −sp | +sp | +sp | +sp | −sp | +sp |
| Helicity | *M* | *P* | *M* | *M* | *P* | *M* | *M* | *M* | *M* |
| $\phi_2$ | −31.70 | 31.70 | −26.39 | −29.70 | 29.70 | −26.33 | −19.89 | 19.89 | −23.75 |
| Conf. | −sc | +sc | −sp | −sc | +sc | −sp | −sp | +sp | −sp |

[a]Conformations are described as anticlinal (ac), anticlinal (ac), antiperiplanar (ap), synperiplanar (sp), and synclinal (sp) based on the torsion angle of $\tau$ and $\phi$. [b]See text for definition of twist angles.

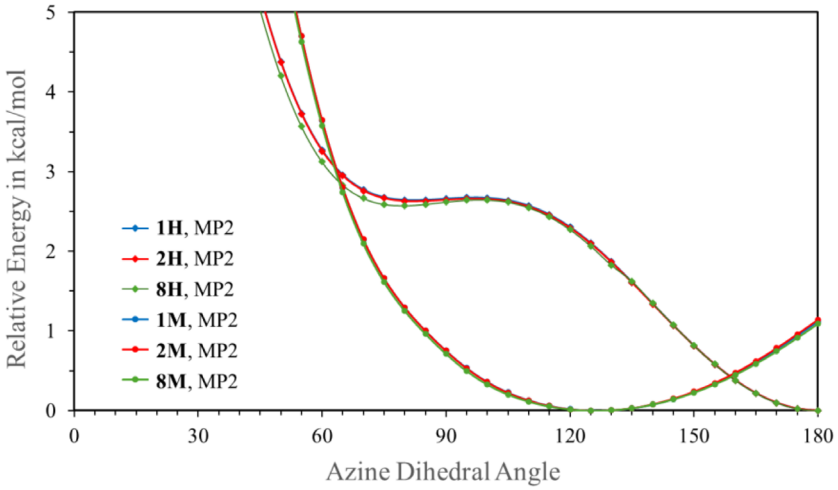


**Figure 3.** Scans of dihedral angle $\tau = \angle$(C═N─N═C) for the benzaldehyde azines **1H**, **2H**, and **8H** (diamonds) and the corresponding acetophenone azines **1M**, **2M**, and **8M** (circles) computed at the MP2(full)/6-311G* level.

accommodate dimeric aggregates and drawings in **Scheme 2** will facilitate the discussion. The edge-hydrogens in Scheme 2 are differentiated by their relative position (*ortho* or *meta*) with regard to the azine functional group and their placement on the inner or outer edge. The inner edge is closer to the long axis of the molecule, i.e., it includes the *ortho* carbon with the low dihedral angle $\angle$(N═C─$C_{ipso}$─$C_{ortho}$). We have already described two paradigms for such side-by-side interactions and, in the current article, the descriptions of the benzaldehyde azines and of the polymorphs **II** of the acetophenone azines reveal two paradigms.

### 3.2.1. Paradigm I: Twisted Spacers and Double T-Contacts

Most of our work focused on acetophenone azines which prefer twisted spacers that place the two arenes in nearly perpendicular planes by combination of an azine twist and disrotatory phenyl twists. This conformation allows for double T-contacts between neighboring azines as shown in **A** in Scheme 2. Crystal structures exemplifying Paradigm I include a wealth of symmetrical (X = Y)[40] and unsymmetrical azines (X ≠ Y)[34] and, in particular, the crystal structures of polymorphs **I** of acetophenone azines **1M**, **2M**, and **8M**.

### 3.2.2. Paradigm II: Trans-Spacer with Phenyl Twists in Butadienes

We recently reported a series of crystal structures with perfectly polar alignment of unsymmetrically disubstituted 1,4-diphenylbuta-1,3-dienes[62] (X = MeO, Y = F, Cl, Br, I). These crystal structures include (ee|ff) double arene contacts between neighboring molecules and manifest Paradigm II. In an (ee|ff) double arene contact, one molecule engages the edges of its two arenes while the other serves as a double face. The lateral offset of the butadiene spacer leads to the optimization of one edge-to-face contact at the cost of the other (**B1** in Scheme 2). However, rotation of the butadiene serving as the double edge around an axis through the center of the E─E bond and conrotatory phenyl twists allow for the optimization of both edge-to-face contacts (**B2** in Scheme 2).[62]

Research Article
doi.org/10.1002/ejoc.202500713



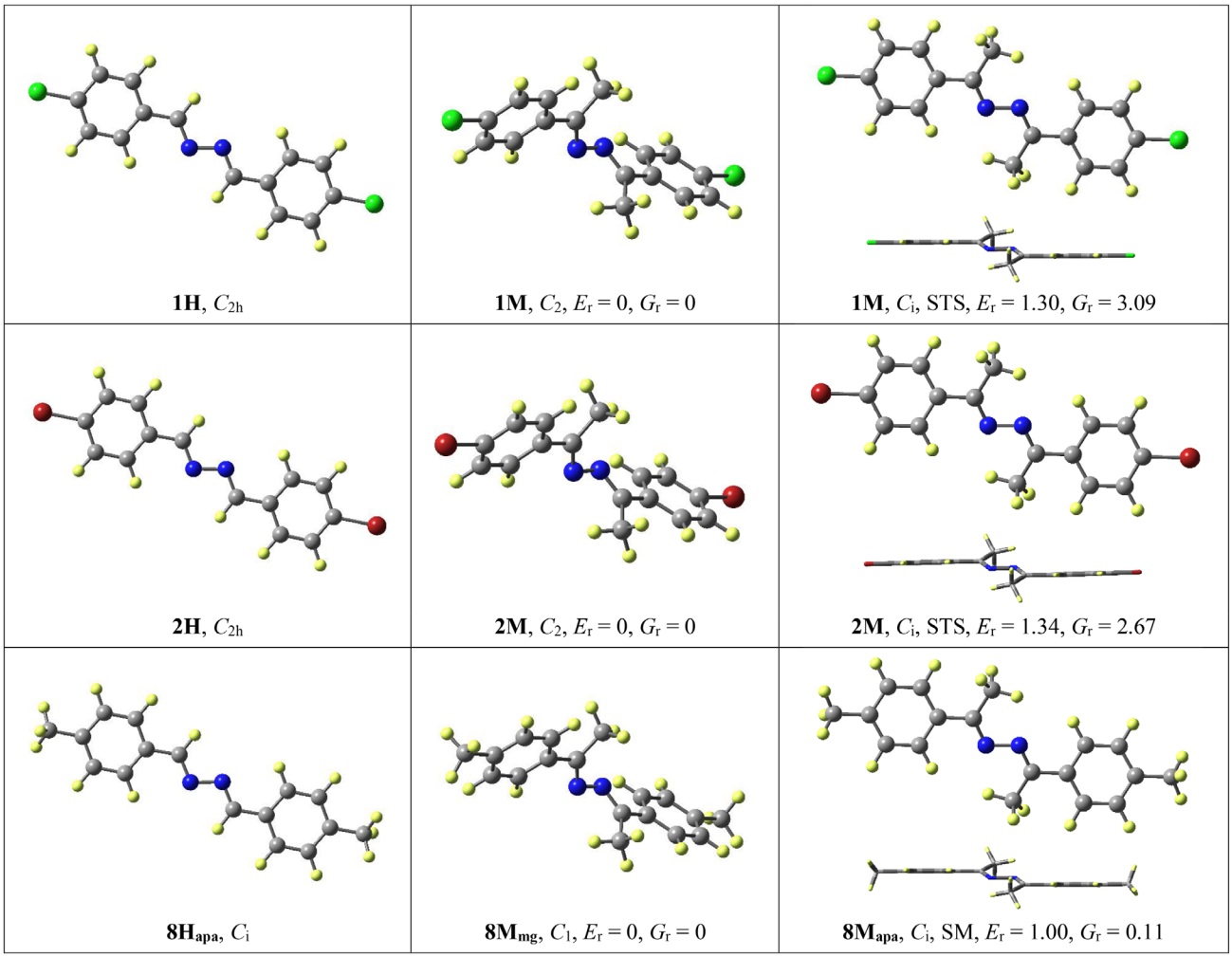


**Figure 4.** Models of pertinent stationary structures of benzaldehyde azines **1H**, **2H**, and **8H** and acetophenone azines **1M**, **2M**, and **8M** optimized at the MP2(full)/6-311G* level.

#### *3.2.3. Paradigm III: Trans-Spacer without Phenyl Twists in 1H and 2H*

Azines **1H** and **2H** exemplify Paradigm III and they form IAMs of a third type (**Figure 5**). Each layer contains stripes of perfectly planar azines held together by double face-to-face stacking interactions. In the second dimension of the IAM, the molecules in neighboring stripes interact via laterally offset edge-to-edge contacts as shown in panel **C** of Scheme 2. The meta hydrogen of the inner edges ($H_{mi}$) engage in hydrogen bonding to azine–N atoms, and each halogen atom engages in bifurcated hydrogen bonding to the proximate very polar C—H bond of the benzaldehyde azine and the *ortho* hydrogen of the outer edge ($H_{oo}$). The halogen atoms also provide for interlayer attraction by way of hydrogen bonding to two meta hydrogens $H_{mo}$ across the IAMs.[50,51]

### 3.3. Crystal Packing of Polymorph 1M-II: Paradigm IV

The IAM of polymorph **1M-II** is of the ideal-shiplap/flat type (Scheme 1), the layer directions are aligned with the crystallographic *a* and *b* axes, and the layers are stacked in the *c* direction. The ideal-shiplap motif of a single IAM is nicely illustrated by the models in **Figure 6**a,b, the interlocking of two such IAMs is illustrated in Figure 6c,d, and the flat nature of the stripes is shown in Figure 6e,f.

#### *3.3.1. Intralayer Interactions: Single T-Contacts Between Neighboring Stripes*

**Figure 7** shows the packing in one IAM of polymorph **1M-II**. Within one stripe, the azine molecules are parallel aligned and all the arenes are parallel stacked (Stripe A). The next neighboring stripe contains azines with different orientation about the *c* direction (Stripe B). The intralayer interaction between molecules in stripes A and B involves single arene–arene T-contacts between their inside arenes $A_i$. The outside arenes $A_s$ decorate the two IAM surfaces and provide interlayer bonding.

Each **1M** molecule is surrounded by six neighboring molecules using five types of interactions **J**, **K**, **L**, **M**, and **N** as illustrated in Figure 7. One perspective is not enough to

Research Article
doi.org/10.1002/ejoc.202500713



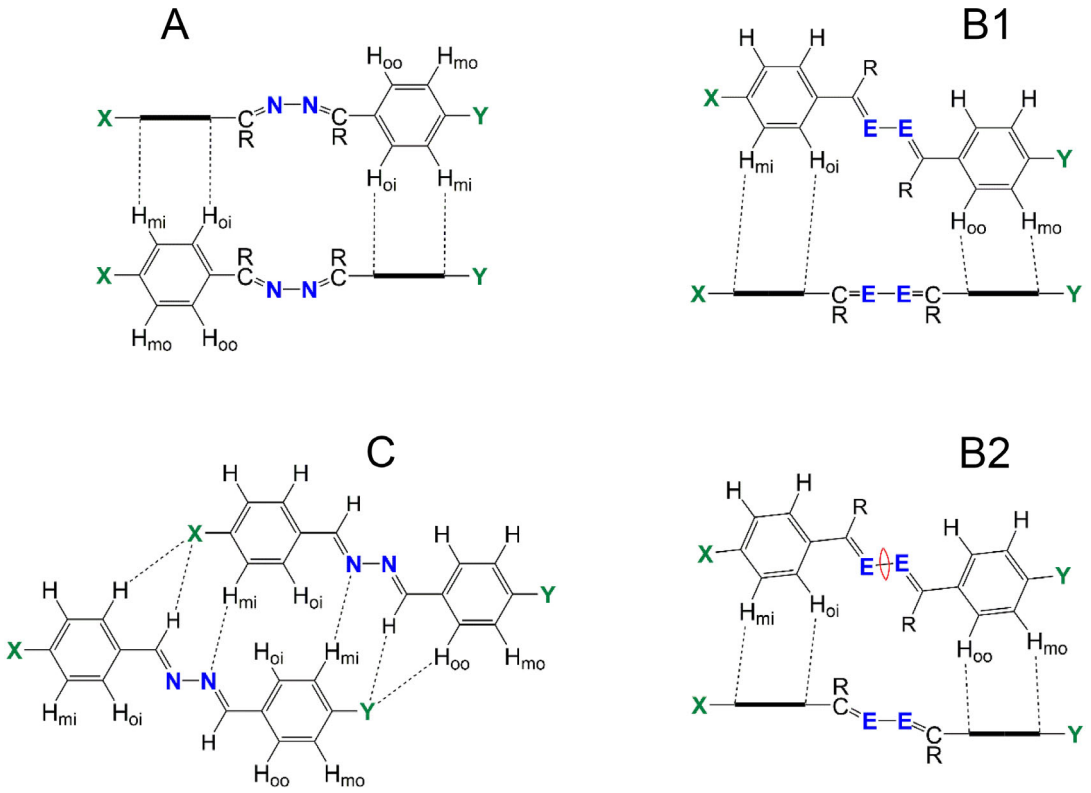


**Scheme 2.** Modalities of double arene–arene contacts between neighboring molecules. A) Double T-contact. B) The (ee|ff) contact in butadienes. C) Laterally offset edge-to-edge contacts in **1H** and **2H**.

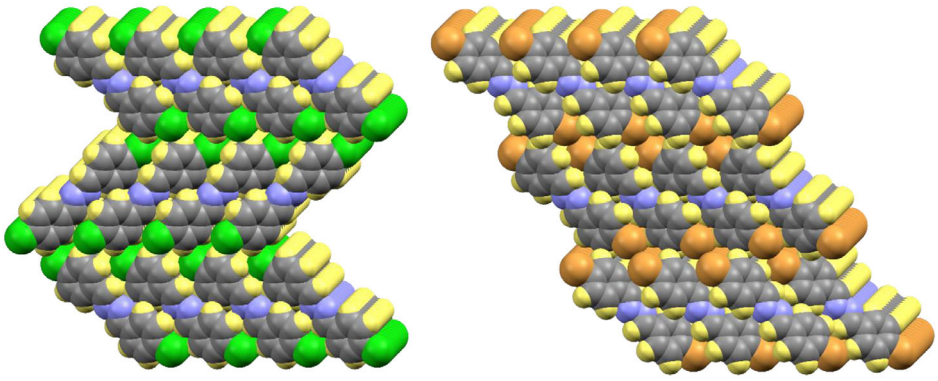


**Figure 5.** Space filling models of crystal architectures in **1H** and **2H**. **1H**, IAM stacking with alternating directions. **2H**, IAM stacking with perfect alignment.

properly appreciate the lateral offset between molecules in neighboring stripes and we provide alternate perspectives in **Figure 8** that clearly distinguish between the inside and outside arenes $A_i$ and $A_s$. The center starred molecule is parallel aligned with **J** in stripe 2 (Figure 8b). It is also interacting with four molecules (**K**, **L**, **M**, and **N**) in stripes 1 and 3. The interactions between the starred molecule and the four neighbors are shown in Figure 8c–f. The inside arene of the starred molecule formally features arene–arene face-to-edge contacts: $A_i$ serves as the face in the contacts with **L** and **M**, and $A_i$ serves as the edge in the contacts with **K** and **N**. It will become clear later that the four interactions are pairwise identical; $E(\mathbf{L}) = E(\mathbf{N})$ and $E(\mathbf{K}) = E(\mathbf{M})$.

### *3.3.2. Chloroarene–Chloroarene Contacts and a New Chloroarene–Azine Synthon*

The longitudinal offset between the molecules in pairs **K** and **M** creates chloroarene–chloroarene contacts, that is, the Cl of one

Research Article
doi.org/10.1002/ejoc.202500713

Chemistry Europe
European Chemical Societies Publishing

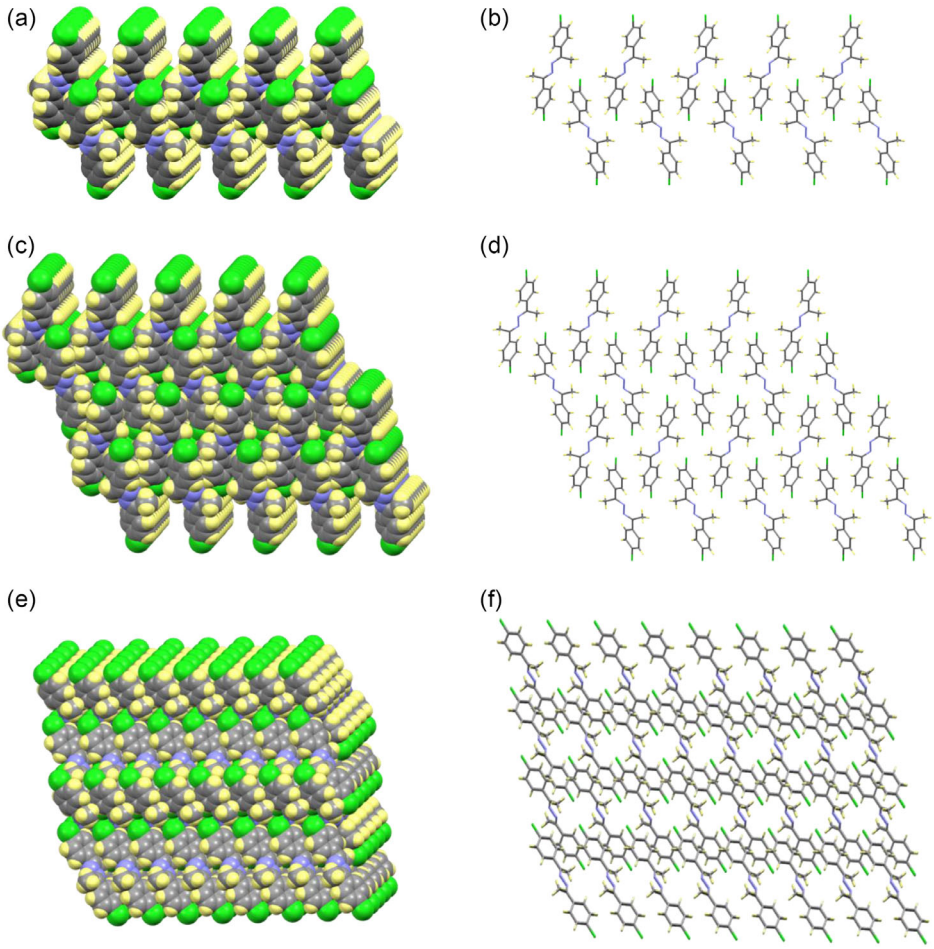


**Figure 6.** Crystal architectures of **1M-II**. Space filling models (left) and tube models (right) are shown. a,b) Single IAM layer viewed down the *a* axis with the *b* axis pointing to the right and *c* axis pointing down. c,d) IAM double layer again viewed down the *a* axis with the *b* axis pointing to the right and *c* axis pointing down. e,f) IAM double layer view down the *b* axis with the *c* axis pointing down and *a* axis pointing to the right.

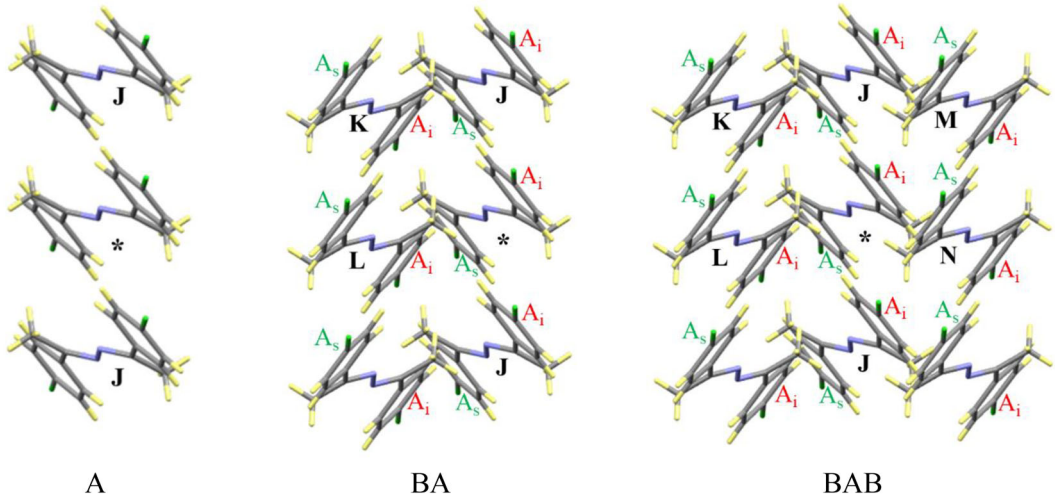


**Figure 7.** Viewed along the *c* direction, stripe A is embedded between two B stripes. Stripes A and B have the same geometry, but one is rotated by 180° around the *b* direction relative to the other. This arrangement results in four strong T-contacts of inside arenes $A_i$; **K** and **L** on one side, **M** and **N** on the other.

Research Article
doi.org/10.1002/ejoc.202500713



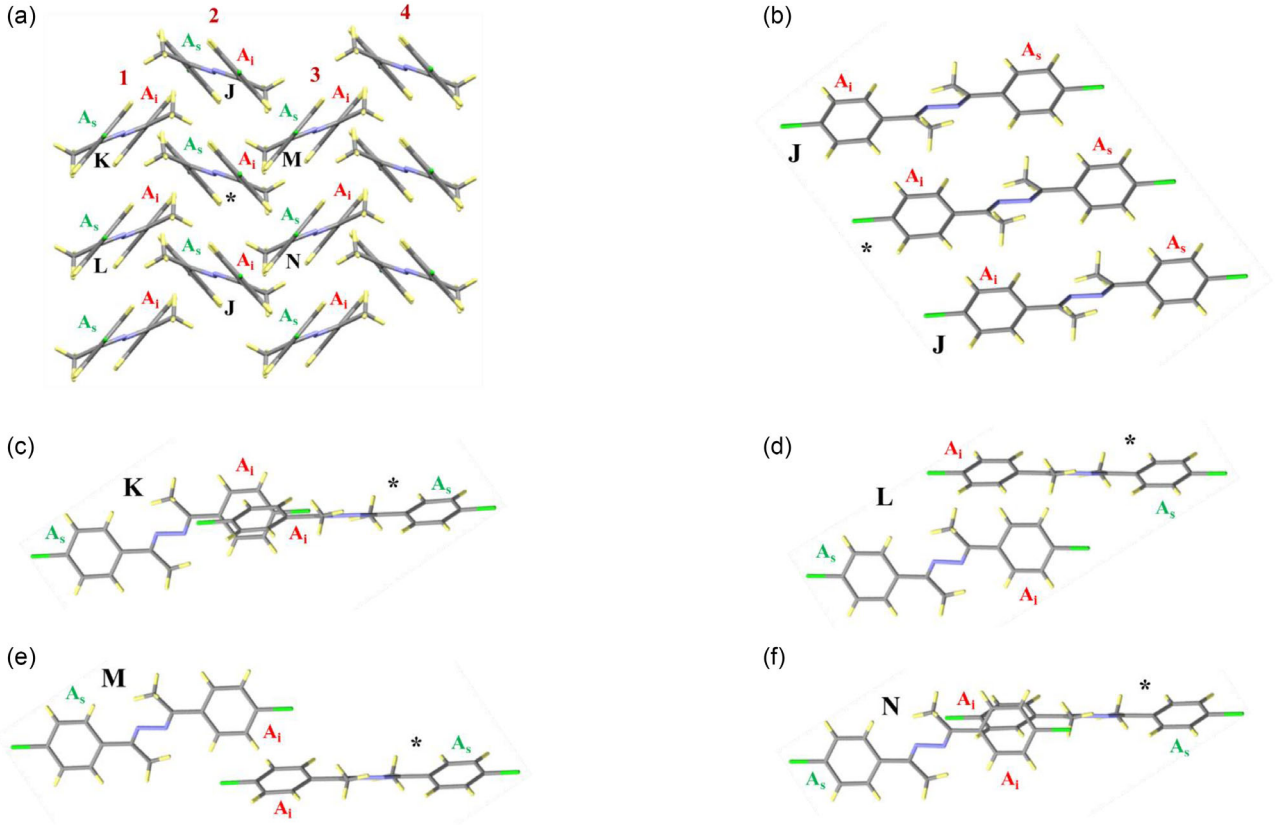


**Figure 8.** The starred molecule **1M** in polymorph **II** interacts with six neighbors using five types of interactions **J**, **K**, **L**, **M,** and **N**. a) IAM structure viewed down the N—N bond axis (*c* axis). b) Stripe 2 is shown along the *b* direction and illustrates **J** type stacking. c,d) The pairing of the starred molecule in stripe 2 with molecules **K** and **L** of stripe 1 is shown along the *b* direction and illustrates **K** and **L** type pairings. e,f) The pairing of the starred molecule in stripe 2 with molecules **M** and **N** of stripe 3 is shown along the *b* direction and illustrates **M** and **N** types pairing.

inside chloroarene is placed above the arene moiety of the other inside chloroarene. Another description of this chloroarene–chloroarene synthon emphasizes that the two edge-$H_e$ atoms of one arene edge -$|H_eH_e|$- engage with an arene face and a chlorine atom to create the (Ar$|H_eH_e|$Cl) contact, which is called an edge chlorine–arene bridging (EClArB) synthon for short.

In contrast, the longitudinal offsets between the molecules in pairs **L** and **N** work in the opposite direction, that is, the two chlorine atoms are far removed from each other and instead one edge-hydrogen ($H_e$) is pointing toward the center of the neighboring arene face. This arrangement places the chlorine atoms of the chloroarene moieties in proximity to azine groups and creating a new arene–azine synthon (**Scheme 3**).

Polymorph **I** featured an arene–azine contact of the type shown on the top left in Scheme 3. The two N atoms of the azine interact with comparable distances with the two edge-Hs of a neighboring arene. The intermolecular arene–azine interaction in polymorph **II** is entirely different in several ways. Both edge-Hs of the neighboring arene still interact with the azine, but the arene is shifted as shown on the bottom left in Scheme 3 to form an **L** pair with one CH···π interaction ($^2$T contact with one C—H, Ar*···$H_e$) and with a single CH···$N_{Az}$ contact resulting in a (Ar$|H_eH_e|N_{Az}$) contact, the edge azine–arene bridging (EAzArB) synthon for brevity. The second major difference concerns the number of neighbors interacting with a specific azine molecule. In polymorph **I**, only one arene is interacting with the azine functional group. In contrast, in polymorph **II**, the azine functional group is engaged by two arenes from different faces, see center of Scheme 3. For the azine functional group in each starred molecule, two identical neighboring molecules belonging to different layers **L** and **L'** are involved in EAzArB pronging interactions (Az*···$H_e$ and Ar*···$H_e$ contacts, Scheme 3 center).

The second intralayer interaction of the starred molecule occurs with pair **M** via chloroarene–chloroarene contact. While polymorph **I** featured an antiparallel face-to-face interaction with two Cl···π contacts,[50] polymorph **II** features an antiparallel face-to-edge interaction (Ar$|H_eH_e|$Cl) with one $H_e$···Cl contact and one $H_e$···π contact and this EClArB interaction is shown on the right in **Scheme 4**. Each starred molecule is involved in two such EClArB interactions: one intralayer interaction (black, **L**) and one interlayer (purple, **L'**).

To complete the discussion of the lattice architecture, one needs to realize the relative offset in the direction perpendicular to the paper plane of Scheme 3. Scheme 4 illustrates ideal T- and L-contacts. In the ideal T-contacts, the planes of the arenes are perpendicular and the edge-Hs point to the center of the face

Research Article
doi.org/10.1002/ejoc.202500713

Chemistry Europe
European Chemical Societies Publishing

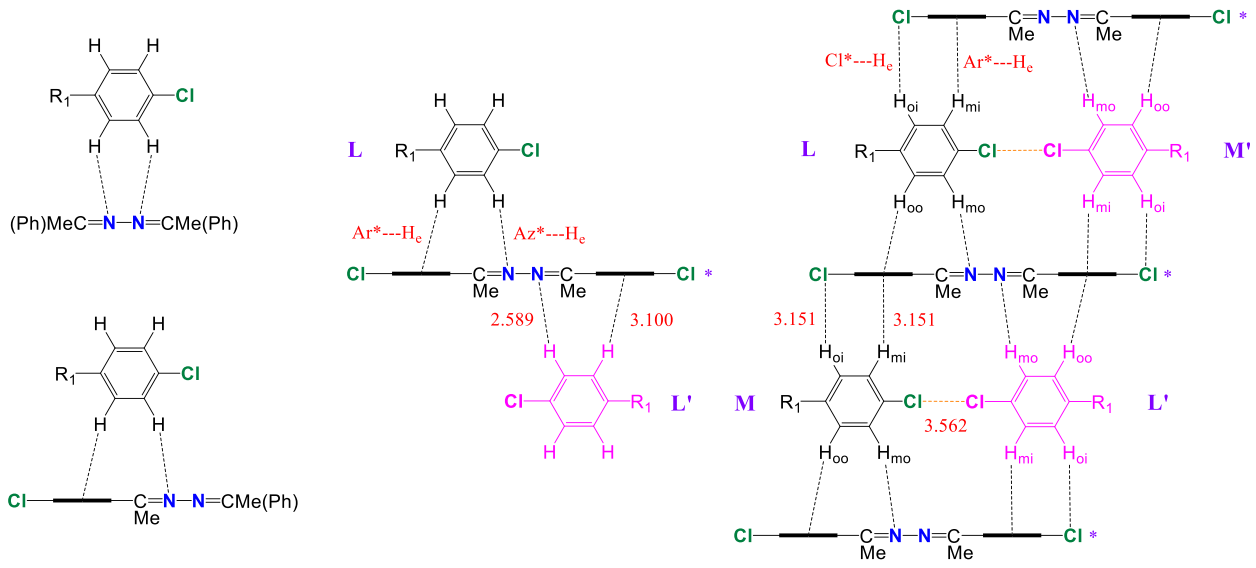


**Scheme 3.** Interaction between edge-hydrogens and azine, arene, and chlorine.

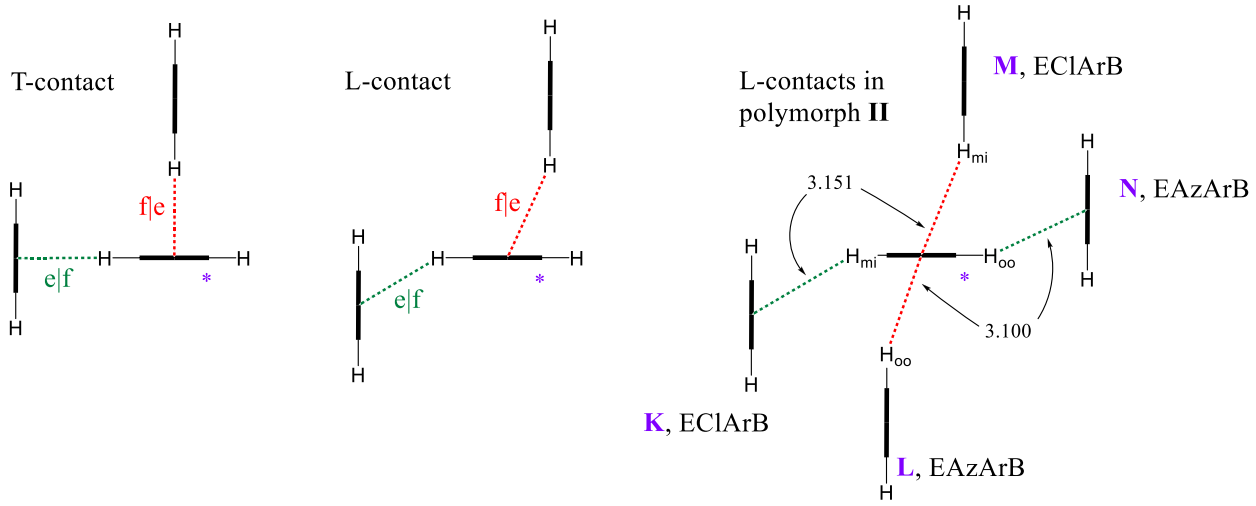


**Scheme 4.** T-contact and L-contact of arene interactions.

arene. On the left in Scheme 4, the starred arene engages as a face (red dash) and as an edge (green dash) with two neighboring arenes. In L-contacts, the planes of the arenes are still more or less perpendicular but the edging arene is offset significantly such that its edge-Hs no longer point to the center of the face arene but rather toward an edge of the face arene as exemplified in the center of the Scheme 3.

In the molecular model shown in **Figure 9**a, the $A_i$ arenes are highlighted in blue and it becomes obvious that the starred $A_i$ engages in four L-contacts as schematically illustrated on the right in Scheme 4 with a view down the long axis of the azine. The arene in the starred molecule in Scheme 4 serves as a face in pairs **M** and **L** and as an edge in the orthogonal direction in pairs **K** and **N**. Pairs **M** and **K** in fact feature exactly the same EClArB interaction and only the roles are switched between facing and edging partners; $d(\mathrm{Ar}|\mathrm{H_e}) = 3.151$ Å. In complete analogy, pairs **L** and **N** feature the same EAzArB interaction with reverse roles; $d(\mathrm{Ar}|\mathrm{H_e}) = 3.100$ Å.

### *3.3.3. Intralayer Interaction Equals Interlayer Interaction in Perfect Shiplap Motif*

We discussed all next-neighbor interactions of one arene $A_i$ of the starred azine, and by our choice, those interactions are intralayer interactions. From this perspective, the other arene of the starred molecule would be considered as a surface arene $A_s$ and its interactions would be interlayer interactions. Because of the ideal-shiplap packing of polymorph **II**, the interlayer interactions are exactly the same as the intralayer interactions. In other words, the $C_i$-symmetry of the azine and the shiplap/flat packing in **II**

Research Article
doi.org/10.1002/ejoc.202500713



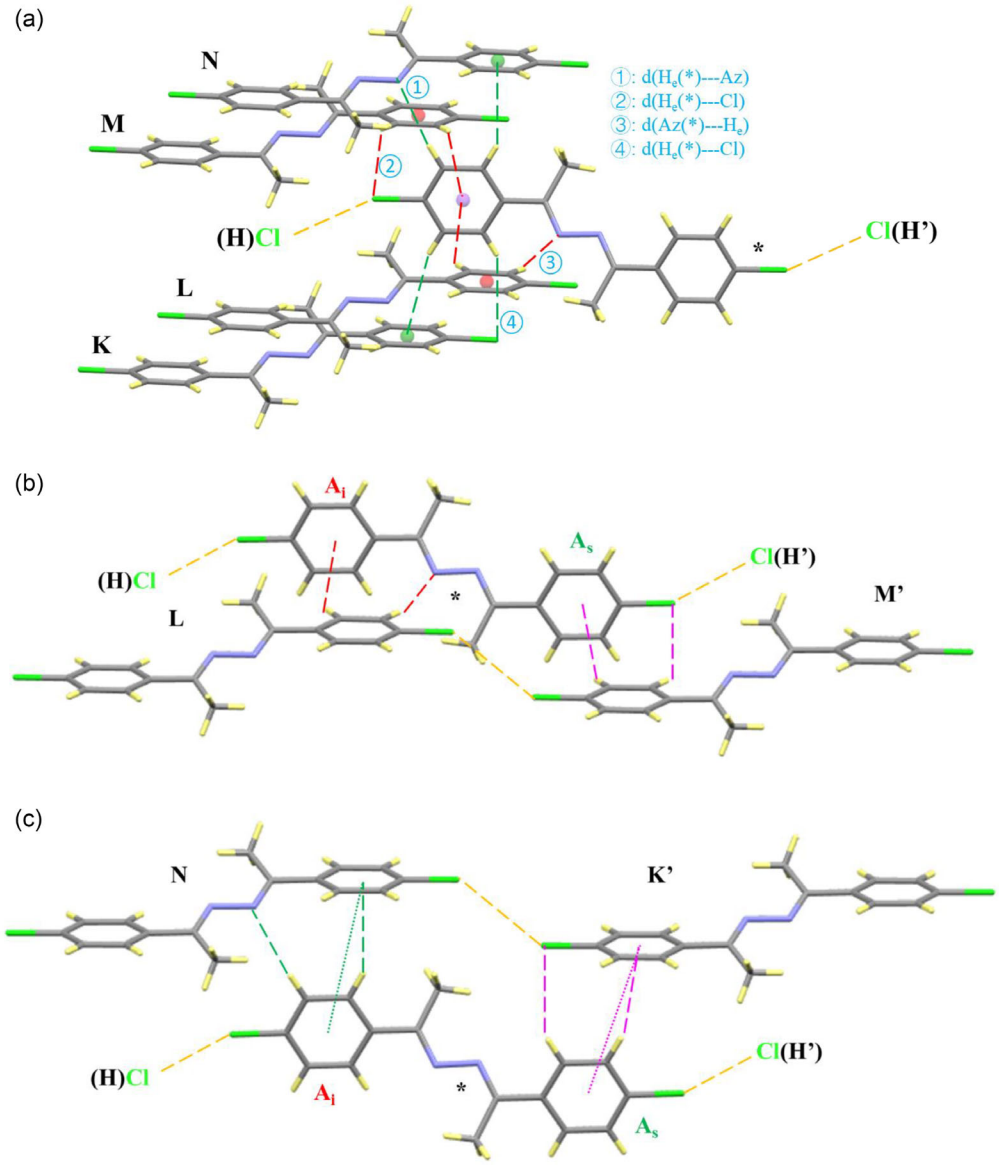


**Figure 9.** a) The starred molecule engages in two e|f (shown in green dash lines) and two f|e (shown in red dash line) interlayer interactions with its $A_i$. b,c) The starred molecule engages in interlayer arene–arene L-contacts with its $A_s$ (pink dash line) in the same fashion as the intralayer interactions (red and green dash line).

guarantees that the two arenes $A_i$ and $A_s$ in each azine engage in the same intermolecular interactions.

We have focused on the intralayer interactions of $A_i$ (Figure 9a) and because of the $C_i$-symmetry, it is now easy to understand the interactions of the other arene $A_s$ of the starred molecule. In Figure 9b, the starred molecule acts as a double face engaging in pairs **L** and **M′**, where **M′** interacts with the $A_s$ of the starred molecule in the same fashion as $A_i$ interacts with **L**. In Figure 9c, the starred molecule acts as a double edge engaging in pairs **N** and **K′**, where **K′** interacts with the starred molecule in the same fashion as **N**.

We are now ready to complete the interaction inventory (**Table 4**). Each azine engages in four EAzArB and four EClArB interactions, with equal contributions to intra- and interlayer interactions. In addition, each azine molecule engages in two identical interlayer Cl···Cl interactions, **H** and **H′**. This Cl···Cl interaction is indicated in Scheme 4 and illustrated in Figure 9b,c with orange dash.

In Table 3, the term e|(f,Cl) describes the interaction **K** of the edge-Hs of $A_i$* with the face and the chlorine atom of the neighboring chloroarene and the term (f,Az)|e describes the interaction **L** of the arene face and azine moiety of $A_i$* with the bridging edge-Hs of the neighboring arene. Intralayer interactions with neighbors **M** and **N**, respectively, are identical to the interactions **K** and **L**, respectively but with reverse roles. The interlayer interactions with neighbors **K′-N′** are the same as interactions with **K-N** with $A_s$* in the role of $A_i$*. In addition, each starred molecule engages both its chlorine atoms in Cl···Cl contacts with interlayer neighbors **H′**.

**Table 4.** Intra- and interlayer interaction inventory for **1M-II**.

| Interaction type[a] | Interacting fragment | Neighboring molecule | | | | |
|---|---|---|---|---|---|---|
| | * | **K** | **L** | **M** | **N** | |
| Intra | $A_i$* | e\|(f,Cl) | (f,Az)\|e | (f,Cl)\|e | e\|(f,Az) | |
| | | **K′** | **L′** | **M′** | **N′** | **H′** |
| Inter | $A_s$* | e\|(f,Cl) | (f,Az)\|e | (f,Cl)\|e | e\|(f,Az) | |
| | Cl($A_i$*) | | | | | Cl($A_s$) |
| | Cl($A_s$*) | | | | | Cl($A_i$) |

[a]See Figure 8 and 9 for definition of intralayer neighbors **K**–**N** and interlayer neighbors **K′**–**N′** and **H′**.

### 3.4. Quantitative Comparison of Intermolecular Interactions of Polymorphs II

#### *3.4.1. Structural Parameters of Intermolecular Interactions*

We measured the structural parameters of the intermolecular interactions, and the results are shown in **Table 5**. The most significant short distances are emphasized by bold red type and contacts of less significance are listed in red type only. In the left-half of Table 5, distances between neighboring Ph−Y moieties are listed for **1M-II** and **2M-II**. The values for **8M-II** are given in analogy to haloazines except for contacts involving methyl groups are measured based on the position of the Me–carbon.

The interactions between proximate antiparallel Ph−Y moieties involve face-to-face interactions in polymorphs **I** but edge-to-face interactions in polymorphs **II**. The face-to-face interactions are well characterized by specification of the distances *d*(Y···Y), the arene–arene distances *d*(Ph···Ph), and the distances *d*(Y···Ph). However, Figure 9c illustrates that the *d*(Ph···Ph) and *d*(Cl···Cl) distances, shown as green (intralayer) and pink (interlayer) dotted lines, are not significant descriptors of edge-to-face interactions, and the same is true for the other azines. Thus, the many numbers as in Table 5 are very similar for all three azines and this similarity corroborates their common crystal architectures. The only significant contacts are the Y*···Y contacts (Y = Cl: 3.562 Å, Y = Br: 3.630 Å, Y = Me: 3.914 Å) which are close to sums of vdW radii. The Y*···Y contact distances in interaction **H** are nearly 0.22 Å (Y = Cl) and 0.09 Å (Y = Br) longer than in the respective polymorphs **I**.

The edge-to-face interactions in polymorphs **II** are only revealed by the *d*($H_e$···Ph) and the *d*($H_e$···Cl/Az) data in the right-half of Table 5. Every type of edge-to-face contact will have one edge-H interacting with an arene face while the second edge-H interacts either with a Y-substituent (**K**, **M**) or an azine-N (**L**, **N**). The edge-H/arene interactions all feature short $H_e$···Ph distances of 3.2 ± 0.1 Å in all of the L-contacts of types **K**, **L**, **M** and **N**. For the **K** and **M** contacts, the $H_e$···Y distances are 3.151 Å (Y = Cl), 3.175 Å (Y = Br), and 3.175 Å (Y = Me), respectively. For the **L** and **N** contacts, the $H_e$···Az distances are 2.589 Å (Y = Cl), 2.640 Å (Y = Br), and 2.590 Å (Y = Me), respectively.

#### *3.4.2. Hirshfeld Analysis of Directionality and Strengths of Intermolecular Interactions*

**Figure 10** shows color-coded illustrations of the inside ($d_i$) and outside ($d_e$) distances mapped on the Hirshfeld surfaces. Red color represents regions with the shortest distances, and distances progressively increase in going from green to blue. The Hirshfeld surface plots for polymorphs **I** of the three azines were reported previously.[40] The 2D-fingerprint plots were also generated for **1M-II**, **2M-II**, and **8M-II** and they are provided in **Figure 11**. The $d_i$ mapped Hirshfeld surfaces inform about the edging arenes while the $d_e$ mapped surfaces illustrate the faces of edge-to-face contacts. The inner edge ($H_{mi}$ and $H_{oi}$) engages in EYArB contacts and the outer edge ($H_{oo}$ and $H_{mo}$) forms EAzArB contacts.

The EYArB synthon can be viewed as simultaneous contacts between an edge-$H_{mi}$ and an edge-$H_{oi}$ with a phenyl face and the halogen Y, respectively. The intense red spots on the Hirshfeld surfaces provide strong evidence that the edge-$H_{mi}$ to phenyl contacts are the crucial component of the EYArB synthon, and the spikes observed in the C···H fingerprint plot reflect the directionality of these contacts (Figure 11).

The EAzArB synthon can be understood as concomitant contacts of the outer edge $H_{oo}$ and $H_{mo}$ atoms with the phenyl face and an azine-N, respectively. In this bridging synthon, both components are equally important as evidenced by the similar intensity of the red regions on the Hirshfeld surfaces. The directionality of these C−$H_{oo}$···Ph and C−$H_{mo}$···N contacts is reflected by the spikes observed in the fingerprint plot for the C···H and N···H contacts in Figure 11.

#### *3.4.3. Aromatic Analyzer Analysis and Strengths of Bidentate Edge-to-Face Contacts*

The strengths of the $^1$T-contacts in the bidentate synthons EYArB and EAzArB were quantified using the aromatic analyzer tool in CSD-Mercury. The analyzer utilizes a machine learning algorithm to develop a model based on molecular descriptors (e.g., atom-atom distance, centroid-to-centroid distance) and DFT energies for all possible orientations of benzene dimer pairs. This model is then used to estimate the interaction strengths. Comprehensive results of our analyses are documented in

**Table 5.** Intermolecular distances characterizing intralayer and interlayer pair interactions in **1M-II**, **2M-II**, and **8M-II**.

| Pair[a] | Ph−Y Contacts | | | | Edge–H Contacts | | | |
|---|---|---|---|---|---|---|---|---|
| **1M-II**[b,c,d,e,f,g] | Cl*···Cl[b] | Ph*···Ph[c] | Cl*···Ph[d] | Ph*···Cl[d] | $H_e$*···Ph[e] | Ph*···$H_e$[e] | $H_e$*···Cl/Az[f] | Cl/Az*···$H_e$[f] |
| J($A_i$*, $A_s$*) | 5.377 | 5.377 | 7.547 | 7.547 | | | | |
| K($A_i$*), K′($A_s$*) | 6.561 | 5.193 | 4.980 | 5.071 | **3.151** | | **3.151** | |
| L($A_i$*), L′($A_s$*) | 8.852 | 5.067 | 6.466 | 6.536 | | **3.100** | | **2.589**[g] |
| M($A_i$*), M′($A_s$*) | 6.561 | 5.193 | 5.071 | 4.980 | | **3.151** | | **3.151** |
| N($A_i$*), N′($A_s$*) | 8.852 | 5.067 | 6.536 | 6.466 | **3.100** | | **2.589**[g] | |
| H($A_i$*), H′($A_s$*) | **3.562** | | | | | | | |
| **2M-II**[h] | Br*···Br | Ph*···Ph | Br*···Ph | Ph*···Br | $H_e$*···Ph | Ph*···$H_e$ | $H_e$*···Br/Az | Br/Az*···$H_e$ |
| J($A_i$*, $A_s$*) | 5.568 | 5.568 | 7.914 | 4.564 | | | | |
| K($A_i$*), K′($A_s$*) | 6.568 | 5.322 | 4.951 | 5.049 | **3.261** | | **3.175** | |
| L($A_i$*), L′($A_s$*) | 9.094 | 5.107 | 6.570 | 6.644 | | **3.144** | | **2.640**[g] |
| M($A_i$*), M′($A_s$*) | 6.568 | 5.322 | 5.049 | 4.951 | | **3.261** | | **3.175** |
| N($A_i$*), N′($A_s$*) | 9.094 | 5.107 | 6.644 | 6.570 | **3.144** | | **2.640**[g] | |
| H($A_i$*), H′($A_s$*) | **3.630** | | | | | | | |
| **8M-II**[i] | Me*···Me | Ph*···Ph | Me*···Ph | Ph*···Me | $H_e$*···Ph | Ph*···$H_e$ | $H_e$*···Me/Az | Me/Az*···$H_e$ |
| J($A_i$*, $A_s$*) | 5.614 | 5.614 | 7.621 | 4.683 | | | | |
| K($A_i$*), K′($A_s$*) | 6.285 | 5.258 | 4.979 | 5.038 | **3.078** | | **3.175** | |
| L($A_i$*), L′($A_s$*) | 8.652 | 5.181 | 6.486 | 6.531 | | **3.139** | | **2.590**[g] |
| M($A_i$*), M′($A_s$*) | 6.285 | 5.258 | 5.038 | 4.979 | | **3.078** | | **3.175** |
| N($A_i$*), N′($A_s$*) | 8.652 | 5.181 | 6.531 | 6.486 | **3.139** | | **2.590**[g] | |
| H($A_i$*), H′($A_s$*) | **3.914** | | | | | | | |

[a]All distances are in Ångström. [b]Cl···Cl distances between a chloroarene pair. [c]Distances between the centers of the arenes in a chloroarene pair. [d]Distances between the chlorine of one chloroarene and the center of the other. [e]Distances between the center of one chloroarene and the closest edge-H of the other. [f]Distances between the Cl atom and the closest edge-H of the other. [g]For **L**, **N**, **L′**, and **N′**, the values "$H_e$*···Az" and "Az*···$H_e$" specify the distance between an edge–H and the closest azine–N atom. [h]Distances for bromoazine **2M-II** are given in complete analogy to chloroazine **1M-II**. [i]Distances for **8M-II** are given in analogy to haloazines except for contacts involving one or two Me groups. In those cases, distances are given based on the position of the Me–carbon.

supporting information and include figures with centroid numbering (Figure S5–S7, Supporting Information for polymorphs **I** and Figure S8–S10, Supporting Information for polymorphs **II**) and tables of scores (Table S4–S6, Supporting Information for polymorphs **I** and Table S7–S9, Supporting Information for polymorphs **II**). Scores in the range 10–7 represent a strong structure-directing and stabilizing aromatic interaction while scores in the range 7–4 represent moderate stabilizing but not structure-defining aromatic interaction.

The scores obtained for the polymorphs **II** show that the EYArB synthons fall within the range 5.9–5.3 while the EAzArB synthons fall within the range 7.2–6.9. This result is in line with the Hirshfeld analysis of the $d_i$ and $d_e$ distances in that the more symmetrically bidentate EAzArB synthon provides for a stronger face-to-edge interaction.

### 3.5. Quantifying Next-Neighbor Interactions and Lattice Energies

#### *3.5.1. Strengths of Next-Neighbor Intermolecular Interactions in Polymorphs II*

Each azine has 10 immediate neighbors overall. The $A_i$* moiety engages in intralayer binding by way of stacking interactions **J**, four face-to-edge interactions **K**, **L**, **M**, and **N**, and the halogen contact **H**. The azine stabilization energy ASE($A_i$*) is given by Equation (1a). We write the term "0.5·2·*E*(**J**)" to reflect that $A_i$* interacts only with one arene $A_i$* (i.e., 0.5) of two **J** neighbors. The energy terms all refer to pair interactions and only one-half of the pair interaction corresponds to the stabilization of the starred azine. Hence, the sum in the curly brackets needs to be multiplied by factor 0.5. Recognizing that $E(\mathbf{L}) = E(\mathbf{N})$ and $E(\mathbf{K}) = E(\mathbf{M})$, the equation simplifies to Equation (1b). Because of the ideal-shiplap architecture azine stabilization energies of both arenes are identical, ASE($A_i$*) = ASE($A_s$*), the overall azine stabilization energy ASE(**II**) is given by Equation (3).

$$\mathrm{ASE}(\mathrm{A_i}*) = 0.5 \times \{0.5 \times 2 \times E(\mathbf{J}) + E(\mathbf{L}) + E(\mathbf{N}) + E(\mathbf{K}) + E(\mathbf{M}) + E(\mathbf{H})\} \quad (1a)$$

$$\mathrm{ASE}(\mathrm{A_i}*) = 0.5 \times \{E(\mathbf{J}) + 2 \times E(\mathbf{L}) + 2 \times E(\mathbf{K}) + E(\mathbf{H})\} \quad (1b)$$

$$\mathrm{ASE}(\mathrm{A_s}*) = 0.5 \times \{0.5 \times 2 \times E(\mathbf{J}) + E(\mathbf{L}') + E(\mathbf{N}') + E(\mathbf{K}') + E(\mathbf{M}') + E(\mathbf{H}')\} \quad (2a)$$

$$\mathrm{ASE}(\mathrm{A_s}*) = 0.5 \times \{E(\mathbf{J}) + 2 \times E(\mathbf{L}') + 2 \times E(\mathbf{K}') + E(\mathbf{H}')\} \quad (2b)$$

$$\mathrm{ASE}(\mathbf{II}) = E(\mathbf{J}) + E(\mathbf{H}) + 2 \times [E(\mathbf{L}) + E(\mathbf{K})] \quad (3)$$

Research Article
doi.org/10.1002/ejoc.202500713



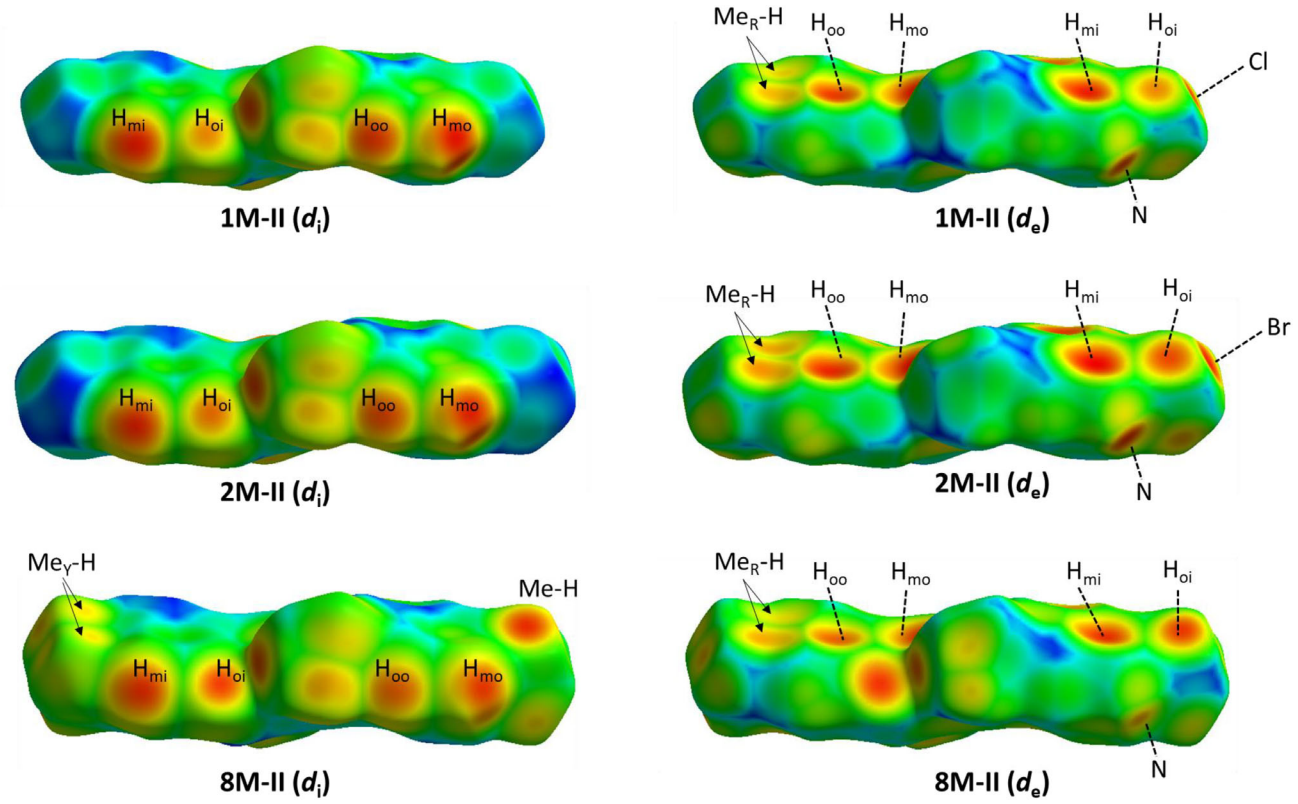


**Figure 10.** Hirshfeld surfaces mapped with the internal ($d_i$, left) and external ($d_e$, right) distances for azines **1M-II**, **2M-II**, and **8M-II**. The distance range chosen for mapping was 1.0–2.5 Å in all cases.

Pairwise interaction energies were computed with CrystalExplorer at the CE-B3LYP level, that is, B3LYP/6-31G(d, p) + D2 for all intra- and interlayer pairs within 3.8 Å of the selected reference molecule in **1M-II**, **2M-II**, and **8M-II**. The computed pair interaction energies are listed in **Table 6** together with the ASE(**II**) values. We also computed the same pair interaction energies with the UNI intermolecular force-field method, and these numbers are also included in Table 6.

The computed data indicate azine stabilization energies ASE in the order **2M-II** < **1M-II** < **8M-II** based on DFT pair interactions while the order **2M-II** ≈ **1M-II** < **8M-II** is predicted with the force-field method. This finding is expected since halogen atoms cause polar bonds and therefore lead to higher lattice energies.

Our results corroborates the discussion of the Hirshfeld surfaces and the aromatic analyzer results and provide quantitative evidence that the interaction energies for pair **L** are about twice as large than for pair **K**. Both of these pairs involve bridging edge-to-face interactions with one edge-H oriented toward an arene center while the other edge-H either points toward an azine-N (**L**, EAzArB synthon) or a halogen atom (**K**, EYArB synthon). Since the edge-H is electron poor, its interaction with the more negatively charged heteroatom should be higher. The term 2·[$E$(**L**) + $E$(**K**)] reflects all four T-contacts and its value is roughly 19.5 ± 2.0 kcal mol$^{-1}$.

The halogen–halogen contacts (**H**) contribute surprisingly little attraction (less than 1.5 kcal mol$^{-1}$) and the $E$(**J**) + $E$(**H**) term is roughly 10.0 ± 1.5 kcal mol$^{-1}$. Hence, the T-contacts clearly dominate crystal stabilization contributing roughly two-thirds of the ASE values.

### 3.5.2. Strengths of Next-Neighbor Intermolecular Interactions in Polymorphs I

Each azine in polymorph **I** of **1M** and **2M** has eight immediate intralayer neighbors (Figure 5 in ref. [40]) and seven interlayer neighbors (Figure 6 in ref. [40]) for a total of 15 next-neighbors. Each azine molecule engages in intralayer binding by way of two stacking interactions **S**, six lateral interactions **Q**, **R**, **T**, **U**, **V**, and **W**. The intralayer azine stabilization energy ASE$_{intra}$ is given by Equation (4a). We write the term "2·$E$(**S**)" to reflect that the starred azine interacts with two such **S** neighbors. Recognizing that $E$(**Q**) = $E$(**T**) and $E$(**V**) = $E$(**W**), the equation simplifies to Equation (4b). The energy terms all refer to pair interactions and only one-half of the pair interaction corresponds to the stabilization of the starred azine. Hence, the sum in the curly brackets needs to be multiplied by factor 0.5. The interlayer azine stabilization energy ASE$_{inter}$ is interesting and contains two terms because the two IAM faces feature different pair interactions. The interlayer interactions of A$_i$* and A$_s$*, respectively, are given by the terms ASE$_{inter}$(A$_i$*) and ASE$_{inter}$(A$_s$*) of Equation (5) and (6), respectively. Recognizing that $E$(**Y**) = $E$(**Y'**) and $E$(**Z$_1$**) = $E$(**Z$_1$'**), Equation (7) collects all interlayer interactions of the starred azine. Thus, the overall azine stabilization energy ASE(**I**) of polymorph **I** can be computed via Equation (8) for **1M** and **2M**.

Research Article
doi.org/10.1002/ejoc.202500713

Chemistry Europe
European Chemical Societies Publishing

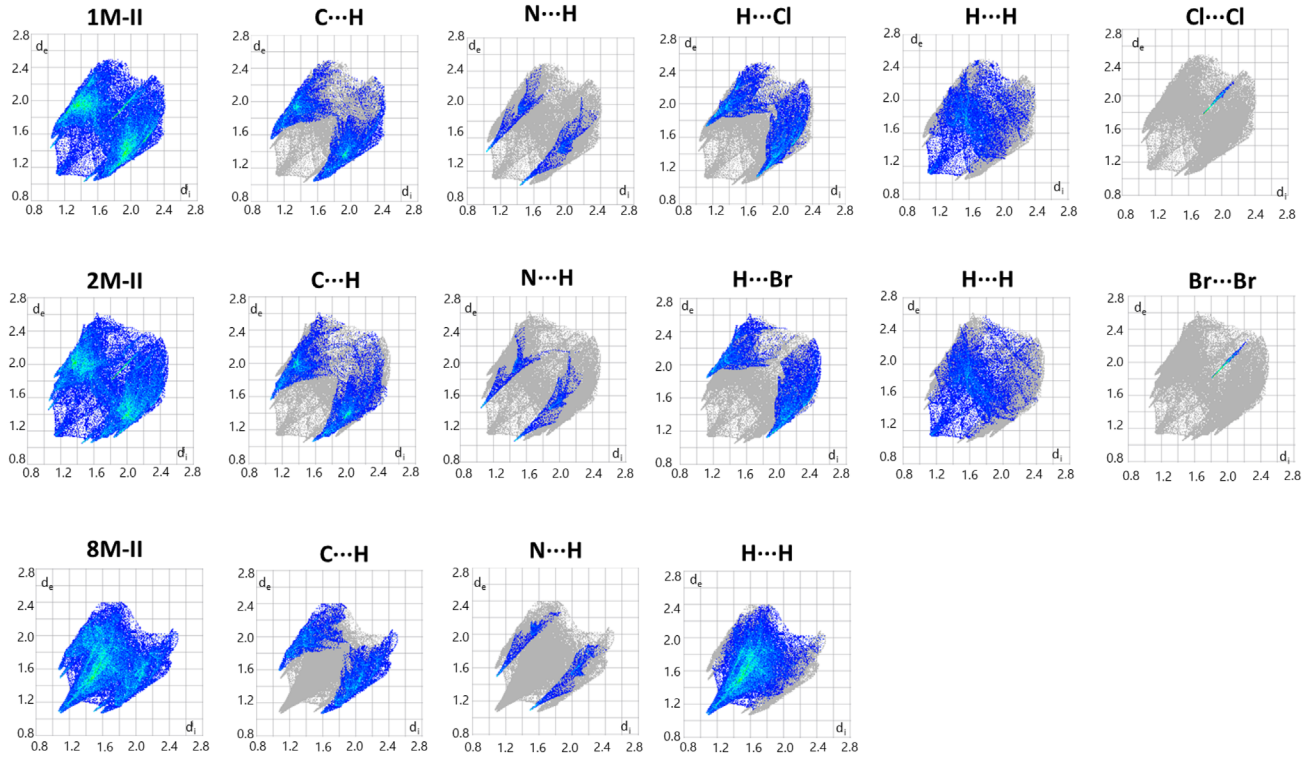


**Figure 11.** 2D-fingerprint plots resolved into C···H, N···H, H···Y, H···H, and Y···Y contacts for the azines **1M-II**, **2M-II**, and **8M-II**.

**Table 6.** Pairwise interaction energies and azine stabilization energies for **1M-II**, **2M-II**, and **8M-II** computed with the CE-B3LYP approach and using the UNI intermolecular force-field.

| Pairs | Energies[a)] | CE-B3LYP | | | UNI intermolecular potentials | | |
|---|---|---|---|---|---|---|---|
| | | **1M-II** | **2M-II** | **8M-II** | **1M-II** | **2M-II** | **8M-II** |
| **J** | $E$(**J**) | −9.4 | −9.7 | −8.0 | −11.0 | −10.6 | −9.7 |
| **L, N, L′, N′** | $E$(**L**) | −6.7 | −7.1 | −6.2 | −6.0 | −6.4 | −6.0 |
| **K, M, K′, M′** | $E$(**K**) | −3.3 | −3.6 | −3.5 | −3.6 | −3.5 | −2.6 |
| **H, H′** | $E$(**H**) | −0.6 | −1.4 | −1.1 | −0.5 | −0.4 | −0.6 |
| | $2 \cdot [E(\mathbf{L}) + E(\mathbf{K})]$ | −20.0 | −21.4 | −19.4 | −19.2 | −19.8 | −17.2 |
| | $E(\mathbf{J}) + E(\mathbf{H})$ | −10.0 | −11.1 | −9.1 | −11.5 | −11.0 | −10.3 |
| | ASE(**II**) | −30.0 | −32.5 | −28.6 | −30.7 | −30.8 | −27.5 |
| | | (94%) | (95%) | (90%) | (86%) | (87%) | (88%) |

[a)]All values in kcal mol$^{-1}$. [b)]Crystal structure analyses at $T = 100$ K for **1M-II** and at $T = 295$ K for **2M-II** and **8M-II**.

$$\mathrm{ASE}_{\mathrm{intra}} = 0.5 \times \{2 \times E(\mathbf{S}) + E(\mathbf{Q}) + E(\mathbf{T}) + E(\mathbf{R}) + E(\mathbf{U}) + E(\mathbf{V}) + E(\mathbf{W})\} \quad (4a)$$

$$\mathrm{ASE}_{\mathrm{intra}} = 0.5 \times \{2 \times E(\mathbf{S}) + 2 \times E(\mathbf{Q}) + E(\mathbf{R}) + E(\mathbf{U}) + 2 \times E(\mathbf{V})\} \quad (4b)$$

$$\mathrm{ASE}_{\mathrm{inter}}(\mathrm{A}_{\mathrm{i}}*) = 0.5 \times \{E(\mathbf{Y}') + E(\mathbf{Z}_1')\} \quad (5)$$

$$\mathrm{ASE}_{\mathrm{inter}}(\mathrm{A}_{\mathrm{s}}*) = 0.5 \times \{E(\mathbf{Y}) + E(\mathbf{X}) + E(\mathbf{Z}_1) + 2 \times E(\mathbf{Z}_2)\} \quad (6)$$

$$\mathrm{ASE}_{\mathrm{inter}} = 0.5 \times \{2 \times E(\mathbf{Y}) + E(\mathbf{X}) + 2 \times E(\mathbf{Z}_1) + 2 \times E(\mathbf{Z}_2)\} \quad (7)$$

$$\mathrm{ASE}(\mathbf{I}) = \mathrm{ASE}_{\mathrm{intra}} + \mathrm{ASE}_{\mathrm{inter}} \quad (8)$$

Pairwise interaction energies were computed as for polymorphs **II** for all pairs within 3.8 Å of the selected reference molecule. The distance for the weak stacking interaction **S** well exceeds 3.8 Å and was included merely for completeness. **Table 7** summarizes the computed pair interaction energies and the resulting ASE(**I**) values along with the respective values computed with the force-field methods.

The computed data indicate azine stabilization energies ASE in the order **2M-I** < **1M-I** based on DFT pair interactions and the same ordering as with polymorphs **II**. However, the force-field

**Table 7.** Pairwise interaction energies and azine stabilization energies for **1M-I** and **2M-I** computed with the CE-B3LYP approach and using the UNI intermolecular force-field.

| Pairs | Energies[a] | CE-B3LYP | | UNI int. potentials | |
|---|---|---|---|---|---|
| | | **1M-I** | **2M-I** | **1M-I** | **2M-I** |
| **S** | $E$(**S**) | −0.3 | −0.4 | −0.3 | −0.4 |
| **V, W** | $E$(**V**) | −8.6 | −8.3 | −10.1 | −9.4 |
| **Q, T** | $E$(**Q**) | −8.8 | −9.3 | −9.2 | −8.9 |
| **R** | $E$(**R**) | −2.9 | −4.5 | −3.2 | −3.7 |
| **U** | $E$(**U**) | −11.4 | −11.7 | −13.3 | −13.0 |
| **X** | $E$(**X**) | −0.8 | −2.4 | −5.8 | −2.4 |
| **Y, Y′** | $E$(**Y**) | 0.0 | −3.0 | −0.9 | −0.7 |
| $\mathbf{Z_1}$, $\mathbf{Z_1}'$ | $E(\mathbf{Z_1})$ | −0.9 | −0.3 | −1.3 | −1.0 |
| $\mathbf{Z_2}$ | $E(\mathbf{Z_2})$ | −2.2 | −1.3 | −1.5 | −2.4 |
| | $ASE_{intra}$ | −24.8 | −26.1 | −27.9 | −27.1 |
| | $ASE_{inter}$ | −3.5 | −5.8 | −6.7 | −5.2 |
| | ASE(**I**) | −28.3 | −31.9 | −34.5 | −32.3 |

[a]All values in kcal mol$^{-1}$. [b]Note that the current values for **1M-I** differ slightly from the data reported in ref. [40] because the current analysis was performed at $T = 100$ K while the previous analysis was based on the $T = 295$ K structure.

method suggests a clear ordering of **1M-I** < **2M-I** while no such difference occurred for polymorphs **II**.

The double T-contacts (**Q**, **T**, **U**) and the arene–azine contacts (**V**, **W**) clearly provide the strongest attraction with binding energies of 8–13 kcal mol$^{-1}$. These large lateral interactions are responsible for $ASE_{intra}$ being at least fourfold larger than $ASE_{inter}$ and thus dominating the overall azine stabilization energies.

### *3.5.3. Pair Binding Approach to Lattice Energies of 1M, 2M, and 8M Polymorphs*

Crystal packing energies were computed for the three pairs of polymorphic molecular crystals (**1M-I** and **1M-II**, **2M-I** and **2M-II**, **8M-I** and **8M-II**). Two approaches were employed to estimate PPEs, and these include azine stabilization energies and lattice energies, and both approaches were implemented using the CE-B3LYP model and the UNI intermolecular force-field method (**Table 8**). The PPE is defined such that positive values indicate a preference for polymorph **I**.

The colorless crystals of polymorphs **1M-I** and **2M-I** can be obtained readily while the yellow crystals of **1M-II** and **2M-II** are formed much less frequently. Assuming that the more stable polymorph also is formed faster, one would expect a positive value for the PPE. Table 8 shows that the force-field method gives positive PPE values using both approaches. The $E_{lat}$ based PPE values computed with the force-field method are 2.7 and 1.8 kcal mol$^{-1}$, respectively, for **1M** and **2M**, respectively.

The design and the interpretation of new crystal architectures necessarily rest on analyses of next-neighbor interactions. This approach to crystal structure analysis is fully warranted if the sum of next-neighbor interactions closely correlates with lattice

**Table 8.** PPEs of polymorphs **I** and **II**.

| Azine | CE-B3LYP[a] | | | UNI intermol. pot.[a] | | |
|---|---|---|---|---|---|---|
| | ASE(**I**) | ASE(**II**) | PPE[b] | ASE(**I**) | ASE(**II**) | PPE[b] |
| **1M** | −28.3 | −30.0 | −3.4 | −34.5 | −30.7 | 3.8 |
| **2M** | −31.9 | −32.5 | −0.7 | −32.3 | −30.8 | 1.5 |
| **8M** | x | −28.5 | x | x | −27.5 | x |
| | $E_{lat}$(**I**) | $E_{lat}$(**II**) | PPE[c] | $E_{lat}$(**I**) | $E_{lat}$(**II**) | PPE[c] |
| **1M** | −30.0 | −31.9 | −1.9 | −38.2 | −35.5 | 2.7 |
| **2M** | −36.8 | −34.2 | 2.6 | −37.5 | −35.6 | 1.8 |
| **8M** | −34.2 | −31.8 | 2.4 | −32.9 | −31.4 | 1.5 |

[a]Azine stabilization energy ASE and lattice energy $E_{lat}$ per azine molecule. [b]Polymorph preference energy, PPE = ASE(**II**) − ASE(**I**). [c]Polymorph preference energy, PPE = $E_{lat}$(**II**) − $E_{lat}$(**I**).

energies. As can be seen from Table 8, this expectation is closely met by the force-field data. Both ASE values and $E_{lat}$ data show PPE(**1M**) < PPE(**2M**) with PPE values positive for **1M** and **2M**.

The CE-B3LYP results deviate from the force-field data. The ab initio derived lattice energies for bromoazine **2M** suggest a clear preference of PPE = 2.68 kcal mol$^{-1}$ which is consistent with the ease of growing crystals of polymorph **I**. However, the data suggest that PPE(**1M**) < PPE(**2M**) and, moreover, that PPE(**1M**) is significantly smaller than zero. There is no easy explanation for the CE-B3LYP results obtained for the chloroazine. At this level we also find much less correlation between next-neighbor interactions and lattice energies.

The pair of polymorphs of **8M** is qualitatively different from the pairs of **1M** and **2M**. Both polymorphs of **8M** are yellow, both polymorphs are formed together in the same crystallization experiment, and both feature shiplap lattice architectures. The lattice energy calculations for **8M** show positive PPE values of 2.4 and 1.5 kcal mol$^{-1}$, respectively, depending on the method (Table 8). Our main interest in **8M** stems from the similarity between **8M-II** and polymorphs **II** of **1M** and **2M**. For these three crystal structures, the force-field derived lattice energies are −35.5 (**1M-II**) ≈ −35.6 (**2M-II**) « −31.4 (**8M-II**) kcal mol$^{-1}$. This ordering reflects the improved crystal stabilization due to halogen-halogen interactions as compared to mere van der Waals attraction between proximate methyl groups.

Differential scanning calorimetry (DSC) can be employed to measure accurate melting points. Since melting points are directly correlated with lattice energies, DSC measurements will allow for an experimental determination of the relative stabilities of the polymorphs. The methodological discrepancies in the calculated relative stabilities of the polymorphs of **1M** and **2M** suggest that experimental clarification is warranted and pertinent.

## 4. Conclusion

We have previously described three paradigms of the supramolecular architectures of diarenes of the types $X_p$—Ph—RC═E—E═CR—Ph—$Y_p$ (E = N: azines; E = CH: butadienes) and all three paradigms formed "flat" IAMs. In flat IAMs, each diarene forms double

Research Article
doi.org/10.1002/ejoc.202500713



arene–arene contacts with an intralayer next-neighbor. Here, we have described the new Paradigm IV for the supramolecular structure of diarene azine materials.

Polymorphs **1M-I** and **2M-I** each contain a racemate of near-$C_2$-symmetric enantiomers with pronounced azine and disrotatory phenyl twists and exemplify Paradigm I. We have now determined the crystal structures of the polymorphs **II** of *para*-chloro- and *para*-bromoacetophenone azines **1M** and **2M**. The azine conformation in polymorphs **II** of azines **1M** and **2M** differ drastically: In polymorphs **II,** the azines are $C_i$-symmetric with *trans*-azine moieties and conrotatory phenyl twists. **1M-II** and **2M-II** are isostructural with polymorph **II** of *para*-methylacetophenone azine **8M**. The crystal structures of these three polymorphs **II** exemplify the new Paradigm IV with longitudinal offset and result in "shiplap/flat" IAMs.

Paradigm IV is a variation of Paradigm II in that the lateral interaction involves edge-to-face arene–arene contacts between molecules with a *trans*-spacer and with phenyl twists but with substantial longitudinal offset. **Scheme 5** illustrates options **D1–D4** for the interaction of a diarene with a *trans*-spacer edging an azine neighbor. The illustrations reflect the placement of the facing arenes in different planes because of the conrotatory phenyl twists. Options **D1–D4** show *ortho* ($H_{oo}$) and *meta* ($H_{mo}$) hydrogens on the outside edge bridging two azine-nitrogens (**D1**, $EArN_2$ synthon), bridging one azine-N and one phenyl center (**D2**, EAzArB synthon), engaging in a bona fide edge-to-face contact (**D3**, $^2$T-synthon), and bridging one phenyl center and substituent Y (**D4**, EYArB synthon).

In polymorphs **II**, an edging diarene engages in one **D2** and one **D4** contact with two different neighbors as illustrated in drawing **E** in Scheme 5. The edging diarene engages its outer edge in an EAzArB contact with one neighboring diarene and its inner edge in an EYArB contact with another neighboring diarene. Note how the phenyl twists allow for the simultaneous

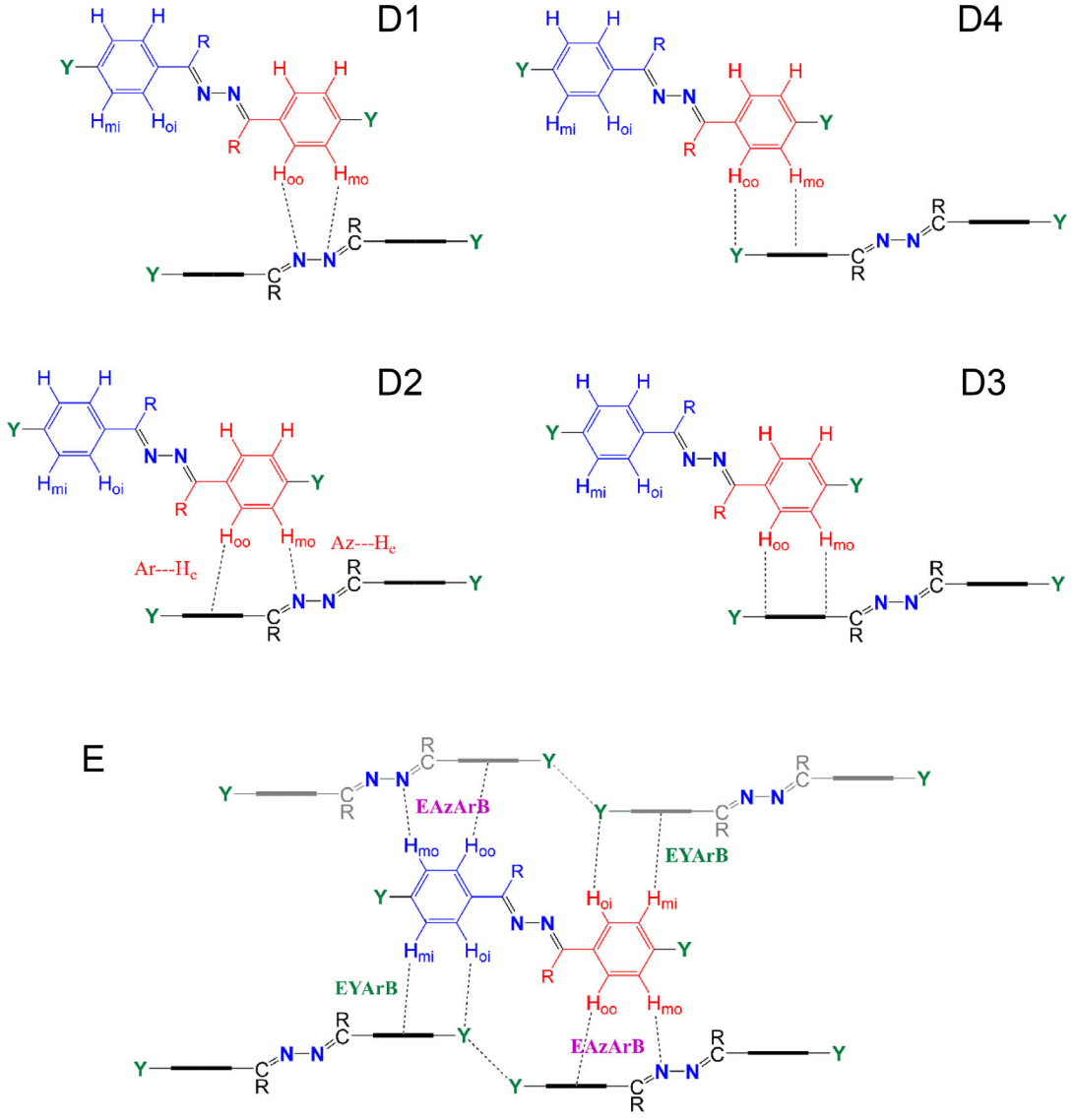


**Scheme 5.** Options **D1–D4** for the interaction of a double face azine with a longitudinally offset double edge azine. Paradigm IV is illustrated by **E.**

optimization of the contact distances of the EAzArB and EYArB synthons. Each phenyl of an edging diarene engages in the EAzArB or EYArB synthon with its outer or inner edge (i.e., interactions with black and grey neighbors).

In the case of **1M**, the different IAM morphologies occur with different molecular shapes of the azines in **I** and **II**. However, there is no direct morphology-stereochemistry relationship because both twisted and nontwisted **8M** azines form shiplap IAMs in polymorphs **A** and **B**.[49] Note also that nontwisted **1H** crystallizes with ideal-flat IAMs.[50]

The $E_{lat}$ based PPE values computed with the force-field method are 2.7, 1.8, and 1.5 kcal mol$^{-1}$ respectively, for **1M**, **2M**, and **8M**, respectively. The relative energies of the $C_i$-structures with trans conformation of **1M**, **2M**, and **8M** compared to the $C_2$-minima are 1.30, 1.34, 1.00 kcal mol$^{-1}$, respectively. Accounting for the conformational preference energies increases the PPEs to 4.0 (**1M**), 3.14 (**2M**), and 2.5 (**8M**) kcal mol$^{-1}$. The conformational preference energies are at least a magnitude smaller than the lattice energies of −35.5 (**1M-II**), −35.6 (**2M-II**), and −31.4 (**8M-II**) kcal mol$^{-1}$.

The interaction inventory analyses reveal two characteristic arene–arene interactions in polymorphs **II**. The bridging EAzArB and EYArB synthons were characterized by a survey of pertinent structure parameters, and their structural significance has been corroborated by analysis of distance mapped Hirshfeld surfaces and the computation of 2D-fingerprint plots. The edge-to-face contacts are the most attractive intermolecular interactions, and we have quantified these interactions via the computed pair interaction energies and the results of aromatic analyzer analysis.

Only one crystal structure is known for the iodo- and fluoroazines **3M**[63] and **7M** (Table 1). Both contain molecules with pronounced azine twists, and neither is isomorphous with **1M-I** and **2M-I**. In the present context it is worthwhile noticing that no polymorphs of **3M** or **7M** with *trans*-azines have been described to date. Our analyses of polymorphs **II** revealed halogen–halogen contacts and these might only be possible for chlorine ($r_{vdW}$ = 1.75 Å) and bromine (1.83 Å) but not for the much smaller fluorine (1.47 Å) and the much larger iodine (1.98 Å).[64]

## Acknowledgements

This work was supported by the Missouri University of Science and Technology and, in part, by a grant from the National Science Foundation #1665487. The authors gratefully acknowledge generous access to the MILL cluster (https://doi.org/10.71674/PH64-N397).

## Conflict of Interest

The authors declare no conflict of interest.

## Data Availability Statement

The Supporting Information contains NMR spectra; selected structural parameters for **1M-II**, **2M-II**, and **8M-II**; centroid numbering and scores obtained from aromatic analyzer analysis; and the Cartesian coordinates of partially optimized unit cell structures of polymorphs **I** and **II** of azines **1M**, **2M**, and **8M**. (28 pages) We have deposited the new crystal structures to CSD and the references include the access information.

**Keywords:** diphenylazines · hirshfeld surface analysis · pair binding energies and lattice energies · polymorph preference energies · supramolecular chemistry

[1] J. Safari, S. Gandomi-Ravandi, *RSC Adv.* **2014**, *4*, 46224.
[2] S. S. Chourasiya, D. Kathuria, A. A. Wani, *Org. Biomol. Chem.* **2019**, *17*, 5498.
[3] L. Jin, Y. Xie, C. Lin, S. Han, D. Shi, H. Yu, *ChemistrySelect* **2024**, *9*, e202304446 (6 p.).
[4] Y. Wang, Z.-Z. Guo, J.-P. Qu, Y.-B. Kang, *Org. Lett.* **2025**, *27*, 1626.
[5] A. Alam, F. U. Rahman, A. A. Elhenawy, A. Ali, *Mini-Rev. Med. Chem.* **2025**, *25*, 425.
[6] G. Kim, J. Yang, N. Nakashima, *Chem. Eur. J.* **2017**, *23*, 11423.
[7] S. Poojary, D. Sunil, D. Kekuda, S. Sreenivasa, *Opt. Mater.* **2018**, *86*, 366.
[8] B. Vercelli, M. Pasini, A. Berlin, J. Casado, J. T. López Navarrete, R. P. Ortiz, G. Zotti, *J. Phys. Chem. C* **2014**, *118*, 3984.
[9] P. Acker, M. E. Speer, J. S. Wössner, B. Esser, *J. Mat. Chem. A.* **2020**, *8*, 11195.
[10] W. Hong, C. Guo, B. Sun, Y. Li, *J. Mater. Chem. C* **2015**, *3*, 4464.
[11] S. Khanra, S. Vassiliades, W. Alves, K. Yang, R. Glaser, K. Ghosh, P. Bhattacharya, P. Yu, S. Guha, *AIP Adv.* **2019**, *9*, 115202.
[12] S. Khanra, T. Cipriano, T. Lam, T. A. White, E. E. Fileti, W. A. Alves, S. Guha, *Adv. Mater. Interfaces* **2015**, *2*, 1500265.
[13] M. Lewis, C. Barnes, R. Glaser, *Acta Cryst. C* **2000**, *56*, 393. 4-Chloroacetophenone-4-Methoxyacetophenone Azine. CCDC Communication, 2000, 143276 (CODRES). CCDC DOI: 10.5517/cc4t2tt.
[14] G. S. Chen, J. K. Wilbur, C. L. Barnes, R. Glaser, *J. Chem. Soc., Perkin Trans.* **1995**, *2*, 2311. ZIFBUL, 1312232, 4-Bromoacetophenone 4-Methoxyacetophenone Azine.
[15] M. Lewis, C. Barnes, R. Glaser, *J. Chem. Crystallogr.* **2000**, *30*, 489. 4-Methoxyacetophenone-4-Iodoacetophenone Azine. CCDC Communication 2001, 165429 (SUXZAM). CCDC DOI: 10.5517/cc5k4f8.
[16] H. Bhoday, M. Lewis, S. P. Kelley, R. Glaser, *ChemPlusChem* **2022**, *87*, e202200224.
[17] H. Bhoday, S. Kelley, R. Glaser, *CrystEngComm* **2023**, *25*, 2175.
[18] H. Bhoday, S. P. Kelley, R. Glaser, *CCDC Commun.* **2020**, 2013773 (XUXDIG).
[19] H. Bhoday, C. L. Barnes, S. P. Kelley, R. Glaser, *CCDC Commun.* **2023**, 2234129 (XUXDIG09).
[20] M. Lewis, H. Bhoday, C. L. Barnes, S. P. Kelley, R. Glaser, *CCDC Commun.* **2020**, 2017223 (NUVPUS).
[21] M. Lewis, H. Bhoday, A. Choudhury, S. P. Kelley, C. L. Barnes, R. Glaser, *CCDC Commun.* **2020**, 2014691 (KUSNEU).
[22] M. Lewis, H. Bhoday, C. L. Barnes, S. P. Kelley, A. Choudhury, R. Glaser, *CCDC Commun.* **2020**, 2017222 (NUVPOM).
[23] R. Glaser, N. Knotts, P. Yu, L. Li, M. Chandrasekhar, C. Martin, C. L. Barnes, *Dalton Trans.* **2006**, 2891.
[24] N. Knotts, R. Glaser, C. Barnes, S. P. Kelley, *CCDC Commun.* **2020**, 2040896 (XUYYEY).
[25] N. Knotts, R. Glaser, C. Barnes, S. P. Kelley, *CCDC Commun.* **2020**, 2040898 (XUYYOI).
[26] N. Knotts, R. Glaser, C. Barnes, S. P. Kelley, *CCDC Commun.* **2020**, 2040895 (XUYYAU).
[27] H. Bhoday, N. Knotts, R. Glaser, *Chem. Eur. J.* **2024**, *30*, e202400182.
[28] N. Knotts, C. Barnes, S. P. Kelley, R. Glaser, *CCDC Commun.* **2022**, 2205422 (NELDAN).
[29] N. Knotts, C. Barnes, S. P. Kelley, R. Glaser, *CCDC Commun.* **2022**, 2205421 (NELCUG).
[30] N. Knotts, C. Barnes, S. P. Kelley, R. Glaser, *Communication* **2022**, 2205420 (NELCOA).
[31] N. Knotts, C. Barnes, S. P. Kelley, R. Glaser, *Communication* **2022**, 2205423 (NELDER).
[32] R. Glaser, N. Knotts, Z. Wu, C. Barnes, *Cryst. Growth Des.* **2006**, *6*, 235.
[33] R. Glaser, N. Knotts, Z. Wu, C. Barnes, *CCDC Commun.* **2006**, 296213 (PAZTIU).

[34] R. Glaser, *Acc. Chem. Res.* **2007**, *40*, 9.
[35] M. Lewis, Z. Wu, R. Glaser, in *Anisotropic Organic Materials - Approaches to Polar Order, ACS Symposium Series* (Eds: R. Glaser, P. Kaszynski), vol. *798*, American Chemical Society, Washington, D.C. **2001**, pp. 97–111.
[36] M. Lewis, R. Glaser, *J. Org. Chem.* **2002**, *67*, 1441.
[37] R. Glaser, G. S. Chen, C. L. Barnes, *J. Org. Chem.* **1994**, *58*, 7446.
[38] G. S. Chen, M. Anthamatten, C. L. Barnes, R. Glaser, *J. Org. Chem.* **1994**, *59*, 4336.
[39] J. Grzegorzek, Z. Mielke, A. Filarowski, *J. Mol. Struct.* **2010**, *976*, 371.
[40] H. Bhoday, K. Yang, S. Kelley, R. Glaser, *CrystEngComm* **2023**, *25*, 4638.
[41] J. S. Chen, M. Anthamatten, C. L. Barnes, R. Glaser, *CCDC Commun.* **1994**, 1207287 (LIKHUI).
[42] H. Bhoday, A. Schuman, S. P. Kelley, R. Glaser, *CCDC Commun.* **2021**, 2056546 (LIKJEU01).
[43] M. Lewis, Ph.D. Thesis, University of Missouri (MU) **2001**.
[44] H. Bhoday, A. Schuman, S. P. Kelley, R. Glaser, *CCDC Commun.* **2020**, 2027206 (HUXMEV).
[45] H. Bhoday, A. Schuman, S. P. Kelley, R. Glaser, *CCDC Commun.* **2023**, 2234130 (LIKJEU02).
[46] R. Glaser, G. S. Chen, M. Anthamatten, C. L. Barnes, *J. Chem. Soc., Perkin Trans.* **1995**, *2*, 1449.
[47] S. P. Kelley, C. L. Barnes, J. Ratchford, K. Yang, N. Corretjer, R. Glaser, *CCDC Commun.* **2018**, 1843926 (WEWMET).
[48] S. Tighdouini, S. Radi, L. Toupet, M. Sirajuddin, T. B. Hadda, M. Akkurt, I. Warad, Y. N. Mabkhot, S. Ali, *J. Chem. Sci.* **2015**, *127*, 2211.
[49] G. S. Chen, M. Anthamatten, C. L. Barnes, R. Glaser, *Angew. Chem. Int. Ed. Engl.* **1994**, *33*, 1081. CCDC Descriptors: PIYYAX, 1235041, polymorph **A** of **2**(Me,Me) in Chen et al.; PIYXOK, 1235039, polymorph **B** of **2**(Me,Me) in Chen et al.
[50] R. Glaser, R. F. Murphy, Y. Sui, C. L. Barnes, S. H. Kim, *CrystEngComm* **2006**, *8*, 372. 4-Chlorobenzophenone Azine. CCDC Communication **2006**, 292918 (GAVCEM01), CCDC DOI: 10.5517/cc9tszv.
[51] R. Glaser, R. F. Murphy, *CrystEngComm* **2006**, *8*, 948.
[52] N. R. L. Correira, T. C. M. Noguiera, A. C. Pinheiro, M. V. N. de Souza, L. R. Gomes, J. N. Low, J. L. Wardell, S. M. S. V. Wardell, *Z. Kristallogr. - Cryst. Mater.* **2018**, *233*, 2017. CCDC Communication 2018, 1551267 (BRBZAL03), CCDC. https://doi.org/10.5517/ccdc.csd.cc1p26wv.
[53] K. Yang, H. Bhoday, R. Glaser, *J. Phys. Org. Chem.*, submitted.
[54] Apex3, *AXScale and SAINT v. 2016.9*, Bruker-AXS, Inc., Madison **2017**.
[55] G. M. Sheldrick, *Acta Cryst. Sect. A. Found. Adv.* **2015**, *71*, 3.
[56] O. V. Dolomanov, L. J. Bourhis, R. J. Gildea, J. A. K. Howard, H. Puschmann, *J. Appl. Cryst.* **2009**, *42*, 339.
[57] S. P. Thomas, P. R. Spackman, D. Jayatilaka, M. A. Spackman, *J. Chem. Theory Comput.* **2018**, *14*, 1614.
[58] C. F. Mackenzie, P. R. Spackman, D. Jayatilaka, M. A. Spackman, *IUCrJ* **2007**, *4*, 575.
[59] A. Gavezzotti, *Acc. Chem. Res.* **1994**, *27*, 309.
[60] C. F. Macrae, I. Sovago, S. J. Cottrell, P. T. A. Galek, P. McCabe, E. Pidcock, M. Platings, G. P. Shields, J. S. Stevens, M. Towler, P. A. Wood, *J. Appl. Crystallogr.* **2020**, *53*, 226.
[61] M. A. Spackman, D. Jayatilaka, *CrystEngComm.* **2009**, *11*, 19.
[62] H. Bhoday, J. Nulsen, S. P. Kelley, R. Glaser, *Chem. Mater.* **2024**, *36*, 8107.
[63] M. Lewis, C. L. Barnes, R. Glaser, *J. Chem. Crystallogr.* **1999**, *29*, 1043.
[64] A. Bondi, *J. Phys. Chem.* **1964**, *68*, 441.

Manuscript received: July 12, 2025
Revised manuscript received: August 22, 2025
Version of record online: